*J. Fluid Mech.* (1995), *vol.* 296, *pp.* 211–245



# Simple shear flows of dilute gas–solid suspensions

By HENG-KWONG TSAO AND DONALD L. KOCH
School of Chemical Engineering, Cornell University, Ithaca, NY 14853, USA

(Received 3 October 1994 and in revised form 8 March 1995)

Kinetic theory and numerical simulations are used to explore the dynamics of a dilute gas–solid suspension subject to simple shear flow. The particles experience a Stokes drag force and undergo solid-body interparticle collisions. Two qualitatively different steady-state behaviours are possible: an ignited state, in which the variance of the particle velocity is very large; and a quenched state, in which most of the particles follow the local fluid velocity. Theoretical results for the ignited state are obtained by perturbing from a Maxwell distribution, while predictions for the quenched state result from consideration of the collision of particles that initially move with the fluid. A composite theory, which includes effects of collisions driven by both the mean shear and the velocity fluctuations, predicts the existence of multiple steady states. Dynamic simulations and calculations using the direct-simulation Monte Carlo method confirm the result that, for certain volume fractions and shear rates, either the quenched or ignited state can be achieved depending on the initial velocity variance.

Simulations are also performed for particles experiencing a nonlinear drag force. Both the theory of rapid granular flow, which neglects drag, and our theory for the ignited state with linear drag predict that the particle velocity variance can grow without bound as $\phi \to 0$, where $\phi$ is the volume fraction. The nonlinear drag force eliminates the divergence and leads to a particle velocity variance that will always decrease with decreasing volume fraction in the limit $\phi \to 0$.

## 1. Introduction

There is an extensive literature on the behaviour of dilute suspensions of solid particles in turbulent and laminar flows in situations where solid-body collisions and all other particle interactions can be ignored (for example Maxey 1987; Squires & Eaton 1990; Alfonso, Gañán-Calvo & Lasheras 1991). On the other hand, considerable study has been devoted to dense rapid granular flows (Savage & Jeffrey 1981; Jenkins & Savage 1983; Lun *et al.* 1984), in which the effects of the fluid phase are neglected. The equations of rapid granular flow have been applied to fluidized beds (see, for example, Sinclair & Jackson 1989) by adding a mean drag due to the fluid phase to the average momentum equation for the particle phase. However, the effect of the gas phase on the kinetic energy contained in the particle velocity fluctuations and on the particle stress is usually neglected.

In this paper, we will consider a sheared gas–solid suspension in the absence of gravity. The volume fraction of the solid phase will be assumed small. However, it will be seen that particle collisions can dramatically alter the behaviour of the suspension even when $\phi \ll 1$. The suspension dynamics are dominated by the drag exerted by the fluid and the solid-body collisions between the particles. Hydrodynamic interactions may be neglected provided that $\phi \ll 1$ and $St \gg 1$. Here, $St \equiv \gamma \tau_v$, $\gamma$ is the shear rate, and $\tau_v \equiv m/(6\pi\mu a)$ is the viscous relaxation time of the particle velocity, where $a$ and

$m$ are the radius and mass of the particle, and $\mu$ is the viscosity of the gas. Hydrodynamic interactions will not be considered in this paper, although we sometimes present results for values of $St$ that are not asymptotically large. The effects of hydrodynamic interactions and large particle volume fractions will be considered in Sangani *et al.* (1995).

Before embarking on our study of the effects of viscous drag on a rapidly sheared gas–solid suspension, it will prove useful to review the theory of rapid granular flow which neglects drag forces. The rapid granular flow is considered analogous to a hard-sphere gas except that a fraction $1-e^2$ of the energy associated with the relative motion of two particles along their line of centres is lost when they collide. Here, $e$ is the coefficient of restitution. The energy associated with the particle velocity fluctuations is determined by a balance of the work done by the mean shear against the effective viscosity of the suspension and the energy dissipated during collisions. The collisional dissipation is proportional to the $O[(1-e^2)mT]$ kinetic energy loss per collision times the $O(\phi^2 a^2 T^{1/2})$ rate of collision, where $T$ is one-third of the mean-square of the particle velocity and is referred to as the granular temperature. The shear work is $\mu_p \gamma^2$, where the particle viscosity $\mu_p$ is obtained from the kinetic theory of gases and is proportional to $T^{1/2}$.

The particle viscosity arises from the transfer of momentum due to the random translation of the particles and from the instantaneous transfer of momentum through a distance $2a$ upon collision of two particles. The former mechanism, referred to as kinetic, dominates in the dilute limit while the latter, known as collisional, is larger in dense suspensions. The growing particle viscosity induced by the collisional stress at high volume fractions causes the temperature to grow with increasing volume fraction for volume fractions larger than about 0.2. However, in the dilute limit, the particle viscosity and shear work are independent of $\phi$ and so the energy balance indicates that the granular temperatures grows with decreasing volume fraction and actually diverges like $\phi^{-2}$ as $\phi \to 0$. This curious behaviour has not been observed experimentally and the physical relevance of the granular theory in this limit has been drawn into question (Lun *et al.* 1984; Campbell 1989, 1990).

At low volume fractions, the dissipation due to viscous drag becomes more important than the dissipation due to inelastic collisions and we consider the effects of viscous drag in detail here. For simplicity, we will consider perfectly elastic particles, $e = 1$. To get a qualitative picture of the results, the reader may now examine some of the results obtained from numerical simulations which include the viscous drag acting on the particles. We have performed both non-equilibrium-molecular-dynamics and Monte Carlo simulations. The steady state of the system is achieved and characterized by the temperature which in turn depends on the volume fraction, Stokes number and the initial velocity variance. The results of the simulations are represented by symbols in figure 7. The lines in the figure are results of a theory that will be explained later.

Two kinds of steady state are observed which are characterized by the relative magnitudes of two timescales: (i) the viscous relaxation time, $\tau_v$, which is the time it takes a particle to relax back to the local fluid velocity after a collision, and (ii) the collision time, $\tau_c$, which is the time between successive collisions of a particle. For a fixed $St$ that is large compared to 1, we are able to obtained a steady state with large velocity variance (compared to $(\gamma a)^2$). This is referred to as an ignited state for which $\tau_v \gg \tau_c$. If the volume fraction is below a critical value which depends on the Stokes number, i.e. $\phi \leqslant \phi_c(St)$, and the initial variance is small enough, the temperature will drop to a value which is small compared to $(\gamma a)^2$. We define this as a quenched state for which $\tau_v \ll \tau_c$. However, we can attain the ignited state even when $\phi \leqslant \phi_c$, if we start

with a large enough variance. In other words, there exist multiple steady states for $\phi \leqslant \phi_c$ and the final steady state depends on the initial variance of the particle velocity.

For a fixed volume fraction, hysteresis in the granular temperature is observed by varying the Stokes number as shown in figure 8. There are two critical Stokes numbers, $St_{c1}$ and $St_{c2}$ where $St_{c2} > St_{c1}$. When $St \geqslant St_{c2}$, only the ignited state exists. When the Stokes number is decreased to the region $St_{c1} \leqslant St \leqslant St_{c2}$, there exist multiple steady states and the final state is determined by the initial velocity variance. For $St \leqslant St_{c1}$, the steady state will be quenched for any initial conditions. $St_{c2}$ varies with $\phi$ and $St_{c1} \approx 5$ independent of volume fraction for $\phi \ll 1$.

In the ignited state the momentum transfer due to particle inertia is far more important than that in the gas phase. Thus, the stress tensor of the particle phase can be obtained from dynamic simulations in a manner analogous to that used for molecular gases. Although the stress tensor is anisotropic in general, the particle phase behaves like a Newtonian fluid as $St \to \infty$. The normal stress differences and the shear-rate dependence of the particle viscosity become significant for values of $St$ close to $St_{c1}$.

In the quenched state, there is an $O(St^3\phi^2)$ contribution to the effective viscosity of the suspension due to the momentum transferred by particle flights following occasional shear-induced collisions. There is also an $O(\phi)$ contribution from the viscous stress acting on the majority of particles whose velocities are equal to the local fluid velocity.

We first used a non-equilibrium-molecular-dynamic-type method to follow the changes in the positions and velocities of $N$ particles in a unit cell with Lees–Edwards periodic boundary conditions as they experienced elastic solid-body collisions and a Stokes drag force. When using dynamic simulations to simulate the quenched state, however, the spatial configuration of the particles in the periodic cell would arrange itself such that the particles would miss one another and no further collisions would occur. This was an artifact of the periodic boundary conditions. To avoid this situation, a more direct numerical construction of the solution to the Boltzmann equation was adopted using the Monte Carlo method of Bird (1970). This technique follows the evolution of the particles' velocity distribution function in time without requiring a precise specification of particle positions. The results for the ignited state from dynamic simulations and the Monte Carlo method were the same.

It is of interest at this point to ask whether there is any experimental evidence for the type of transition observed in our simulations. Although it is not possible to obtain dilute sheared suspensions with negligible gravitational effects on Earth, we can compare our result qualitatively to turbulent pressure-driven vertical tube flows of dilute gas–solid suspensions. In experiments with fine particles, it is observed that the particles respond primarily to the gas-phase turbulence (Elghobashi & Abou-Arab 1983), while more massive particles experience velocity fluctuations induced by interparticle collisions (Louge, Mastorakos & Jenkins 1991). These observations are consistent with our results showing that an ignited state occurs for particles with higher Stokes numbers. While these experiments contain a number of complicating factors, including gas-phase turbulence as well as the possibility of gravitationally induced instabilities, it is clear from the work of Louge *et al.* (1991) that shear plays a dominant role at least for the larger particles.

Quenched and ignited states have also been predicted for a somewhat different physical setting (Goldreich & Tremain 1978). The particle velocities in Keplerian shear of a planetary ring are determined by shear-induced particle collisions as well as gravitational and centrifugal forces. (Drag forces are negligible.) If the orbital velocity

is much less than the collision frequency, then a particle will attain a new orbit before it has an opportunity to collide and transmit its momentum to another particle and one obtains a state with a low velocity variance. In the opposite limit, one obtains a highly agitated state.

In the following sections, we will explain the simulation results summarized above using a kinetic theory. The background for the kinetic theory is introduced briefly in §2. Instead of solving the nonlinear Boltzmann equation directly, a moment method is adopted in §3. Based on an assumed functional form (second-order Hermite polynomials) for the velocity distribution function, the rate of change of the second moments due to collisions can be expressed in terms of second moments only. The collisions are driven by the fluctuations of the particle velocity with respect to the mean (variance-driven collisions) and by the difference in the mean velocities corresponding to the positions of the two particles (shear-induced collisions). Two stable solutions for the temperature are found. One corresponds to the ignited state and the other is the quenched state with zero variance. Neglecting shear-induced collisions leads to a prediction that every particle will move with the local fluid velocity in the quenched state. We study the effects of shear-induced collisions on the quenched state in §4. In §5, a theory which includes both variance-driven and shear-induced collisions in the collision integral is used to derive a $St_c$–$\phi_c$ diagram which displays the regions of ignited, quenched, and multiple steady states observed in the simulations. In §6, the effects of nonlinear drag on the quenched–ignited transition are considered. The results show that the divergence of granular temperature in the limit $\phi \to 0$ is eliminated due to nonlinear drag.

## 2. Background for the kinetic theory

We shall consider a dilute suspension of solid particles in a gas undergoing a steady homogeneous simple shear flow with the fluid velocity $\boldsymbol{u}$ given by

$$\boldsymbol{u} = \boldsymbol{G}\cdot\boldsymbol{r}, \quad G_{ij} = \gamma\delta_{ix}\delta_{jy}, \tag{2.1}$$

where $x$ and $y$ correspond to the flow and gradient directions respectively. The state of the dilute gas–solid suspension is characterized by the one-particle distribution function $F(t, \boldsymbol{r}, \boldsymbol{v})$ where $\boldsymbol{v}$ is the particle velocity. The normalization of the distribution is $n = \int F \mathrm{d}^3v$, where $n = n(t, \boldsymbol{r})$ is the number density. The average, $\langle \Psi \rangle$, of a function $\Psi = \Psi(\boldsymbol{v})$ is given by

$$\langle \Psi \rangle = \frac{1}{n}\int \Psi F \mathrm{d}^3v. \tag{2.2}$$

For example, the mean mass density $\rho_s$ is $mn$, the mean of the particle velocity $\boldsymbol{v}$ is $\langle \boldsymbol{v} \rangle$, and the particle temperature is $\langle C^2 \rangle/3$. It is convenient to introduce the fluctuating velocity $\boldsymbol{C}$, which is defined as the velocity relative to the mean, $\boldsymbol{C} \equiv \boldsymbol{v} - \langle \boldsymbol{v} \rangle$; through $\langle \boldsymbol{v} \rangle$, it is a function of $\boldsymbol{r}$. The distribution function $f$ depends on the fluctuating velocity $\boldsymbol{C}$ rather than $\boldsymbol{v}$ and is defined by $\int F \mathrm{d}^3v = \int f \mathrm{d}^3C$. If the suspension is nearly homogeneous and its behaviour varies slowly with time, the velocity distribution function can be described by a Boltzmann equation (Chapman & Cowling 1970) of the form

$$-\frac{\partial f}{\partial \boldsymbol{C}}\boldsymbol{C}:\frac{\partial}{\partial \boldsymbol{r}}\langle \boldsymbol{v} \rangle + \frac{\partial}{\partial \boldsymbol{C}}\cdot(\dot{\boldsymbol{v}} f) = \frac{\partial_c f}{\partial t}. \tag{2.3}$$

Equation (2.3) states that, at steady state, the collisional rate of change of the distribution function for the fluctuating velocity is balanced by the rate of change of $f(\boldsymbol{C})$ due to particle motion with respect to the mean velocity field (streaming) and the rate of change of $f(\boldsymbol{C})$ due to external forces acting on the particles. In the present application, the external force is viscous drag and so it is important to write the acceleration $\dot{\boldsymbol{v}}$ inside the divergence operator.

In the absence of the gravitational forces, the equation of motion for the particle will be approximated as

$$\dot{\boldsymbol{v}} = -(\boldsymbol{v}-\boldsymbol{u})/\tau_v. \tag{2.4}$$

It should be noted that the primary effect of gravitational forces would be to change the mean particle velocity. Velocity fluctuations are induced by gravity only in polydisperse suspensions (Kumaran, Tsao & Koch 1994) or through hydrodynamic interactions (Koch 1990). The velocity fluctuations produced by both these mechanisms have been found to be weak compared with the fluctuations induced by shearing.

In (2.4), we have neglected the history dependence of the drag force. The ratio of the Basset history term to the steady Stokes drag is $O(a/(\nu t)^{1/2})$, where $\nu = \mu/\rho_f$ is the kinematic viscosity of the gas and $t$ is the timescale over which changes in particle velocity occur. Taking $t$ to be the collisional time $\tau_c = a\phi^{-1}/\langle \boldsymbol{C}^2\rangle^{1/2}$, the history term is $O(Re_T^{1/2}\phi^{1/2})$ smaller than the Stokes drag term. Here, $Re_T = 2\rho_f\langle \boldsymbol{C}^2\rangle^{1/2}a/\mu$. This provides an upper bound on the importance of history effects, which decay more rapidly than indicated by the Basset formula for $\tau_c > \nu/\langle \boldsymbol{C}^2\rangle$ or $Re_T > \phi$ (Mei & Adrian 1992).

We have also neglected interparticle hydrodynamic interactions in writing (2.4). The leading effect of hydrodynamic interactions is an $O(\phi^{1/2})$ enhancement of the drag on a particle (Brinkman 1947). In addition, for particles of large Stokes number, the change in the velocities of the particles due to lubrication forces will be small, $O[\log(a/\lambda)/St_T]$ (Koch 1990), where $\lambda$ is the mean-free path of the gas. The Stokes number $St_T \equiv 2\rho_p\langle \boldsymbol{C}^2\rangle^{1/2}a/9\mu$ is based on the root-mean-square velocity of the particle. Here $\rho_p$ is the density of the particle.

Under steady simple shear flow, the number density and second moments of the velocity distribution are constant, and the contracted third moments vanish due to symmetry. As a consequence, the average velocity of the particles follows the velocity of the fluid. This result can also be easily understood from the momentum equation for the particle phase. For a steady simple shear, the equation reduces to the condition that the mean drag due to the gas phase is equal to zero. Therefore, $\langle \boldsymbol{v}\rangle = \boldsymbol{u}$ and $\partial\langle \boldsymbol{v}\rangle/\partial \boldsymbol{r} = \boldsymbol{G}$. Using (2.4) for the viscous drag force acting on the particle, the Boltzmann equation (2.3) can be rewritten as

$$-\frac{\partial f}{\partial C_x}C_y\gamma + \frac{\partial}{\partial C_i}\left(-\frac{C_i}{\tau_v}f\right) = \frac{\partial_c f}{\partial t}. \tag{2.5}$$

The order of magnitude of the convection and drag terms on the left-hand side are, respectively, $\gamma f$ and $f/\tau_v$. The collision term on the right-hand side is $O(\Delta f/\tau_c)$ where $\Delta f$ is the deviation from the Maxwellian. The order of magnitude of $\tau_c$ is determined by the collision mechanism, which may be variance driven or shear induced. Variance-driven collisions dominate and $\tau_c \ll \tau_v$ in the ignited state. For a variance-driven collision, the mean free path is $a\phi^{-1}$ and the relative velocity scales with $\langle \boldsymbol{C}^2\rangle^{1/2}$. As a consequence, the collision time is $\tau_c \sim O(a\phi^{-1}/\langle \boldsymbol{C}^2\rangle^{1/2})$. If $\langle \boldsymbol{C}^2\rangle^{1/2}/\gamma a \gg \phi^{-1}$ and $St_T\,\phi \gg 1$, we will have the situation $\tau_c \ll \gamma^{-1} \ll \tau_v$. When this criterion is satisfied, the collision term on the right-hand side of (2.5) controls the velocity distribution function,

which is therefore close to the Maxwellian. However, in the quenched state, where most of the collisions are induced directly by the mean shear, the relative velocity is $O(\gamma a)$ and the collision frequency is $O(\gamma a \pi a^2 n)$. As a consequence, $\tau_c$ is $O(\gamma\phi)^{-1}$ and we have the conditions $\tau_c \gg \tau_v \gg \gamma^{-1}$ if $St \gg 1$. Neglecting the collision term altogether, we obtain $f = n\delta(\boldsymbol{C})$ in the quenched state.

The balance law for $\Psi(\boldsymbol{C})$ may be obtained from the Boltzmann equation. Multiplication of (2.3) by $\Psi$ and subsequent integration over $\mathrm{d}^3\boldsymbol{C}$ yields

$$\left\langle \frac{\partial \Psi}{\partial \boldsymbol{C}} \boldsymbol{C} \right\rangle : \frac{\partial}{\partial \boldsymbol{r}} \langle \boldsymbol{v} \rangle - \left\langle \dot{\boldsymbol{v}} \cdot \frac{\partial \Psi}{\partial \boldsymbol{C}} \right\rangle = \frac{\partial_c \langle \Psi \rangle}{\partial t}. \tag{2.6}$$

The right-hand side of (2.6) represents the rate of change of $\langle \Psi \rangle$ due to collisions. Although the collisions conserve particle mass, momentum, and mechanical energy, $\Psi = m\boldsymbol{C}$ or $\frac{1}{2}m\boldsymbol{C}^2$ are not conserved because these quantities differ from the momentum and energy by factors of order $m\gamma a$ and $m(\gamma a)^2$, respectively. Thus, $\partial_c \langle \boldsymbol{C}^2 \rangle / \partial t$ is non-zero but is small, $O(\gamma^3 a^2 \phi)$. In the ignited state, $|\boldsymbol{C}| \approx |\boldsymbol{v}| \gg \gamma a$ and we can neglect this small collisional source. The collision terms will also lead to a transport of momentum and energy; the momentum and energy transferred from one particle to another in a collision is instantaneously transported through a distance $2a$. However, in the dilute limit, the mean-free path $a\phi^{-1}$ is much larger than $2a$ and the collisional transport is much smaller than the transport due to the random translational motion of the particles. This is directly analogous to the situation in a dilute hard-sphere gas.

Then, by taking $\Psi$ in (2.6) to be $\rho_s \boldsymbol{C}\boldsymbol{C}$, the balance laws for the components of the stress tensor are given by

$$(G_{ik} P_{kj} + G_{jk} P_{ki}) + \frac{2}{\tau_v} P_{ij} = \frac{\partial_c (P_{ij})}{\partial t}, \tag{2.7}$$

where $P_{ij} = \rho_s \langle C_i C_j \rangle$, and $\rho_s = nm$ is the density of the suspension. By summing the balance laws for $\langle P_{xx} \rangle$, $\langle P_{yy} \rangle$, and $\langle P_{zz} \rangle$, the energy balance can be obtained without determining the full velocity distribution function:

$$-P_{xy}\gamma = \rho_s \langle \boldsymbol{C}^2 \rangle / \tau_v. \tag{2.8}$$

Equation (2.8) simply states that the work done by the shear transforms the energy associated with the mean motion into fluctuating energy and viscous drag dissipates the fluctuating energy into heat.

In a collision between a pair of elastic particles, the velocities $\boldsymbol{v}_1'$ and $\boldsymbol{v}_2'$, of the particles after collision are related to those, $\boldsymbol{v}_1$ and $\boldsymbol{v}_2$, before collision and to the unit vector $\boldsymbol{k}$, directed from the centre of the first particle to the centre of the second at impact. The velocity change in a collision is given by

$$(\boldsymbol{C}_r' - \boldsymbol{C}_r) = (\boldsymbol{v}_r' - \boldsymbol{v}_r) = (-1)^r (\boldsymbol{g} \cdot \boldsymbol{k})\, \boldsymbol{k}, \tag{2.9}$$

where $r = 1, 2$ and $\boldsymbol{g} \equiv \boldsymbol{v}_1 - \boldsymbol{v}_2$. The total change $\Delta\Psi$ in a collision is defined as $\Delta\Psi \equiv \Psi_1' + \Psi_2' - \Psi_1 - \Psi_2$. For example, the changes in the second moments during an elastic collision are given by

$$\Delta(C_i C_j) = [2(\boldsymbol{g} \cdot \boldsymbol{k})^2 k_i k_j - (k_i w_j + k_j w_i)(\boldsymbol{g} \cdot \boldsymbol{k})], \tag{2.10}$$

where $\boldsymbol{w} \equiv \boldsymbol{C}_1 - \boldsymbol{C}_2 \equiv (\boldsymbol{v}_1 - \boldsymbol{v}_2) - \Delta\boldsymbol{u}$ with $\Delta\boldsymbol{u} \equiv \boldsymbol{u}_1 - \boldsymbol{u}_2$.

To obtain the stress tensor for the particle phase from the balance laws for the second moments, the collisional change in the second moments, i.e. the right-hand side

of (2.7), must be known. The rate of change of the property $\Psi$ due to collisions can be evaluated as the integral over all possible collisions of the change in $\Psi$ in a particular collision multiplied by the frequency of such a collision, i.e.

$$n\frac{\partial_c\langle\Psi\rangle}{\partial t}=\frac{1}{2}\int_{g\cdot k>0}(\Delta\Psi)f^{(2)}(\boldsymbol{C}_1,\boldsymbol{C}_2)(\boldsymbol{g}\cdot\boldsymbol{k})\,\mathrm{d}\Gamma, \tag{2.11a}$$

where we have introduced the abbreviated notation

$$\mathrm{d}\Gamma=4a^2\,\mathrm{d}\boldsymbol{k}\,\mathrm{d}\boldsymbol{C}\,\mathrm{d}\boldsymbol{C}_1. \tag{2.11b}$$

Here the complete pair distribution $f^{(2)}$ is defined such that

$$f^{(2)}(\boldsymbol{C}_1,\boldsymbol{r}_1,\boldsymbol{C}_2,\boldsymbol{r}_2)\,\mathrm{d}\boldsymbol{C}_1\,\mathrm{d}\boldsymbol{r}_1\,\mathrm{d}\boldsymbol{C}_2\,\mathrm{d}\boldsymbol{r}_2$$

is the number of pairs of particles that at time $t$ are located in the volume elements $\mathrm{d}\boldsymbol{r}_1$ and $\mathrm{d}\boldsymbol{r}_2$ centred at $\boldsymbol{r}_1$ and $\boldsymbol{r}_2$ with velocities in the volume elements $\mathrm{d}\boldsymbol{C}_1$ and $\mathrm{d}\boldsymbol{C}_2$ at $\boldsymbol{C}_1$ and $\boldsymbol{C}_2$ in velocity space. Consequently, the number of collisions per unit volume per unit time is $f^{(2)}(\boldsymbol{C}_1,\boldsymbol{C}_2)(\boldsymbol{g}\cdot\boldsymbol{k})\,\mathrm{d}\Gamma$. In order to relate the complete pair distribution function at collision to the one-particle velocity distribution function, we adopt the assumption of molecular chaos. Thus, we ignore the possible correlation in the velocities of colliding particles, so that the pair distribution function for two colliding particles is a product of the single-particle velocity distribution, i.e. $f^{(2)}(\boldsymbol{C}_1,\boldsymbol{C}_2)=f_1(\boldsymbol{C}_1)\cdot f_2(\boldsymbol{C}_2)$. This assumption is valid when the volume fraction is low and the Stokes number is high.

Since the stress tensor is related to the second moment of the fluctuating velocities, it is convenient to express $\Delta(C_i\,C_j)$ in terms of the relative fluctuating velocity $\boldsymbol{w}$ instead of the relative velocity $\boldsymbol{g}$. As a result, the collisional change of the second moments is given as

$$n\frac{\partial_c\langle C_i\,C_j\rangle}{\partial t}=\frac{1}{2}\int_{g\cdot k>0}\Delta(C_i\,C_j)f_1f_2(\boldsymbol{g}\cdot\boldsymbol{k})\,\mathrm{d}\Gamma=\Xi_1+\Xi_2+\Xi_3, \tag{2.12}$$

where

$$\Xi_1=\int_{g\cdot k>0}(\boldsymbol{w}\cdot\boldsymbol{k})[2(\boldsymbol{w}\cdot\boldsymbol{k})k_i\,k_j-(w_i\,k_j+w_j\,k_i)]f_1f_2(\boldsymbol{w}\cdot\boldsymbol{k})\,\mathrm{d}\Gamma, \tag{2.13}$$

$$\Xi_2=\int_{g\cdot k>0}2[(\Delta\boldsymbol{u}\cdot\boldsymbol{k})^3k_i\,k_j]f_1f_2\,\mathrm{d}\Gamma, \tag{2.14}$$

and

$$\Xi_3=\int_{g\cdot k>0}(\Delta\boldsymbol{u}\cdot\boldsymbol{k})\{3[(\boldsymbol{w}\cdot\boldsymbol{k})^2+(\boldsymbol{w}\cdot\boldsymbol{k})(\Delta\boldsymbol{u}\cdot\boldsymbol{k})]k_i\,k_j$$
$$-[2(\boldsymbol{w}\cdot\boldsymbol{k})+(\Delta\boldsymbol{u}\cdot\boldsymbol{k})](w_i\,k_j+w_j\,k_i)\}f_1f_2\,\mathrm{d}\Gamma. \tag{2.15}$$

In the ignited state, $|\Delta\boldsymbol{u}|\ll|\boldsymbol{w}|$ and $\Xi_2+\Xi_3$ is $O(\gamma a/\langle C^2\rangle^{1/2})$ smaller than $\Xi_1$. On the other hand, $|\Delta\boldsymbol{u}|\gg|\boldsymbol{w}|$ in the quenched state and $\Xi_1+\Xi_3$ can be neglected.

In order to evaluate the collision integrals for the second moments and obtain the stress tensor, the velocity distribution function must be known. However, owing to the mathematical complexity of the nonlinear Boltzmann equation, it is not possible to obtain an exact analytic solution. Therefore, the velocity distribution function will be assumed to be a truncated Hermite expansion in the ignited state and the coefficients

in the expansion will be determined by satisfying the second-moment balance equations. In the quenched state, the velocity distribution will be determined as a perturbation to a delta function.

## 3. Ignited state ($\tau_c \ll \tau_v$)

In the ignited state, a particle typically flies 'randomly' with a small change in its velocities caused by drag during the flight from one collision to the next. To understand the ignited state better, it will be helpful to review the energy balance controlling the root-mean-square fluctuating velocity $\langle C^2\rangle^{1/2}$. The order of magnitude of the particle velocity fluctuations at steady state can be determined by the balance between the energy input in shearing the suspension and the energy dissipation due to drag. The shear work is approximately equal to $\mu_p \gamma^2$ while the viscous dissipation is $6\pi\mu an\langle C^2\rangle$. Here $\mu_p$ is the particle-phase shear viscosity and can be estimated from the kinetic theory of dilute gases to yield $\mu_p \sim \rho_s a\phi^{-1}\langle C^2\rangle^{1/2}$. The energy balance then shows that the velocity fluctuation is $\langle C^2\rangle^{1/2} \sim (St/\phi)\gamma a$. Thus the criterion for a collision-dominated velocity distribution is $St = \gamma\tau_v \gg 1$. We might have expected intuitively that the criterion for the ignited state would depend on the volume fraction as well as the Stokes number and that the system would be quenched for sufficiently small volume fractions. However, the criterion for the existence of the ignited state is independent of $\phi$ and this suggests the possibility of multiple steady states for sufficiently small $\phi$. This conjecture will be confirmed in §5.

For a collision-dominated system, we expect the velocity distribution to be Maxwellian to leading order. The shear will cause an $O(St^{-1})$ deviation from the Maxwellian, which gives rise to the shear viscosity of the particle phase, and an $O(St^{-2})$ deviation, which corresponds to the normal stress difference.

### 3.1. *Variance-driven collisions*

To obtain an approximate analytical solution of Boltzmann's equation, a perturbation scheme based on the assumption that the fluctuating velocities of the particles are Maxwellian to leading order has usually been adopted. Examples include the Chapman–Enskog expansion (Chapman & Cowling 1974) and the method of moments (Grad 1949). In addition to these two standard methods, the velocity distribution function can be assumed to be an anisotropic Maxwellian (Goldreich & Tremaine 1978; Jenkins & Richman 1988).

In this paper, a moment method is employed to derive the collisional change in the second moments of the velocity fluctuation. In general, the velocity distribution function $f$ can be written as

$$f = f_M(1+\Phi), \tag{3.1}$$

where $\Phi$ is a measure for the deviation of $f$ from the local Maxwellian distribution

$$f_M = \frac{n}{(2\pi T)^{3/2}}\exp\left(-\frac{C^2}{2T}\right). \tag{3.2}$$

The deviation from the Maxwellian $\Phi(t, \boldsymbol{r}, \boldsymbol{C})$ can be expanded in a series of orthogonal functions. Usually, the expansion functions will be tensors, such as tensor Hermite polynomials or tensor Sonine polynomials. Thus,

$$\Phi(\boldsymbol{r}, t, \boldsymbol{C}) = a_i^{(1)} h_i^{(1)} + \frac{a_{ij}^{(2)}}{2!} h_{ij}^{(2)} + \frac{a_{ijk}^{(3)}}{3!} h_{ijk}^{(3)} + \ldots. \tag{3.3}$$

Here $h^{(n)}_{i_1\ldots i_n}$ is a tensor polynomial of rank $n$ in three-dimensional space and the orthogonality of the tensor polynomials is given by

$$\langle h^{(n)}_{i_1\ldots i_n} h^{(n)}_{j_1\ldots j_n}\rangle_M = n!\,\Delta^{i_1\ldots i_n}_{j_1\ldots j_n}, \tag{3.4a}$$

where

$$\Delta^{i_1\ldots i_n}_{j_1\ldots j_n} = 1, \tag{3.4b}$$

when $\{i_1,\ldots,i_n\}$ is a permutation of $\{j_1,\ldots,j_n\}$ and zero otherwise. $\langle\cdot\rangle_M$ means an average over velocity space weighted by the Maxwellian. The expansion coefficients $a^{(n)}_{i_1\ldots i_n}$ are determined by

$$a^{(n)}_{i_1\ldots i_n} = \langle h^{(n)}_{i_1\ldots i_n}\Phi\rangle_M = \langle h^{(n)}_{i_1\ldots i_n}\rangle. \tag{3.5}$$

Since no spatial gradient of a moment can occur for simple shear flow, the odd moments need not to be considered. In addition, we assume that the influence of the fourth and higher moments on the stress tensor is small. Thus the deviation $\Phi$ can be approximated by

$$\Phi = \frac{a^{(2)}_{ij}}{2!} h^{(2)}_{ij}, \tag{3.6a}$$

with

$$a^{(2)}_{ij} = \frac{\langle C_i C_j\rangle}{T} - \delta_{ij} \quad \text{and} \quad h^{(2)}_{ij} = \frac{C_i C_j}{T} - \delta_{ij}. \tag{3.6b}$$

Upon changing variables from $\boldsymbol{C}_1$ and $\boldsymbol{C}_2$ to $\boldsymbol{w}$ and $\boldsymbol{q} \equiv (\boldsymbol{C}_1+\boldsymbol{C}_2)/2$, noting that $\mathrm{d}\boldsymbol{C}_1\,\mathrm{d}\boldsymbol{C}_2 \equiv \mathrm{d}\boldsymbol{w}\,\mathrm{d}\boldsymbol{q}$, and carrying out the integrations in (2.12) and (2.13) with the second-order Hermite expansion (3.6*a*, *b*), the collisional rate of change of the stress tensor due to variance-driven collisions is given by

$$\left(\frac{\partial_c P_{ij}}{\partial t}\right)_i = -\omega^{(2,2)}\hat{P}_{ij} - \frac{\tilde{\omega}^{(2,22)}}{\sqrt{2p}}\{\hat{P}_{ik}\hat{P}_{kj} - \tfrac{1}{3}\mathrm{tr}\,(\hat{P}_{ik}\hat{P}_{kj})\}, \tag{3.7}$$

where $\hat{P}_{ij}$ is the traceless part of the stress tensor, e.g. $\hat{P}_{ij} = P_{ij} - p\delta_{ij}$. Here $p$ is the particle pressure defined as $p \equiv \rho_s T$. The subscript $i$ on the collisional change of the stress tensor indicates that this approximation is valid for the ignited state. The pair distribution function $f_1 f_2$ in (2.13) contains terms that are linear and quadratic in the perturbation $\Phi$. These lead to the terms in (3.7) that are linear and quadratic in the second moment. The ratio $\tilde{\omega}^{(2,22)}/\omega^{(2,2)}$ is a measure of the relative size of the quadratic and linear terms.

Note that (3.7) contains quadratic terms in the collision integral due to the product of the linear terms in the velocity distribution but no contribution from the quadratic terms in the velocity distribution. The quadratic terms (fourth moments) in the velocity distribution do not contribute to the collision integral for the second moment owing to the orthogonality of the tensor Hermite polynomials.

Herdegen & Hess (1982) show that the collision coefficients $\omega^{(2,2)}$ and $\tilde{\omega}^{(2,22)}$ of (3.7) can be expressed in terms of the collision integrals $\Omega^{(p,q)}$ evaluated by Chapman & Cowling (1970):

$$\omega^{(2,2)} = \tfrac{8}{5} n\Omega^{(2,2)}, \tag{3.8}$$

$$\tilde{\omega}^{(2,22)} = \tfrac{4}{5} n(\tfrac{2}{7}\Omega^{(2,3)} - \Omega^{(2,2)}), \tag{3.9}$$

where, for hard spheres of diameter $2a$, $\Omega^{(p,q)}$ are given by

$$\Omega^{(p,q)} = \left(\frac{T}{\pi}\right)^{1/2} \frac{(q+1)!}{2}\, Q^{(p)}. \tag{3.10}$$

with $$Q^{(p)} = \left[1 - \frac{1}{2}\frac{1+(-1)^p}{1+p}\right]\pi(2a)^2. \tag{3.11}$$

In the kinetic theory of gases, two molecules separated by a distance $r$ with a repulsive force given by a power law $F \sim r^{-5}$ are termed Maxwell molecules. $\tilde{\omega}^{(2,22)}$ vanishes for Maxwell molecules and one only has the first, linear term on the right-hand side of (3.7) for this special interaction potential. For hard spheres $\tilde{\omega}^{(2,22)}$ is non-zero but it is substantially smaller than $\omega^{(2,2)}$.

On substituting (3.7) for the collisional change of the stress tensor into (2.7), a closed set of nonlinear equations for the second moments is derived from Boltzmann's equation with the help of the moment method. In this equation, terms nonlinear in the shear rate due to the presence of a velocity gradient (shear flow) as well as nonlinearities emerging from the collision term are taken into account. The relevant linear and nonlinear collision integrals have been expressed in terms of Chapman–Cowling $\Omega$-integrals and can be evaluated for various collision models (Herdegen & Hess 1982).

### 3.2. *Stress tensor*

Let us now introduce the following non-dimensional time, position and velocity:

$$\tilde{t} = \gamma t, \quad \tilde{\boldsymbol{r}} = \boldsymbol{r}/a, \quad \tilde{\boldsymbol{u}} = \boldsymbol{u}/(\gamma a). \tag{3.12}$$

The dimensionless temperature, pressure and pressure tensor are defined as

$$\tilde{T} = T/(\gamma a)^2, \quad \tilde{p} = p/[\rho_s(\gamma a)^2], \quad \tilde{\boldsymbol{P}} = \boldsymbol{P}/[\rho_s(\gamma a)^2]. \tag{3.13}$$

All the equations that follow will use non-dimensional variables, and, for clarity, we shall henceforth omit the tildes.

Before solving the closed nonlinear equations, (2.7) and (3.7), for the stress tensor, it will be helpful to have an order of magnitude analysis of each term in the nonlinear equations. The convection and drag terms on the left-hand side of (2.7) are $O(T)$ and $O(St^{-1}T)$, respectively. According to the energy balance, the collision time $\tau_c$ and granular temperature $T$ are found to be $O(St^{-1})$ and $O(St/\phi)^2$, respectively. In addition, $P_{xy}$ is $O(St^{-1}T)$. There are no convection terms in the equations for $P_{yy}$ and $P_{zz}$. Therefore, a balance of the drag and collision terms gives $O(St^{-2}T)$ normal stress differences. As a result, the linear and quadratic terms involving the normal pressure $P_{ii}$ on the right-hand side of the equation for $\partial_c(P_{ii})/\partial t$ are $O(St^{-1}T)$ and $O(St^{-3}T)$ respectively. The quadratic terms involving the shear stress $P_{xy}$ are $O(St^{-1}T)$. The linear and quadratic terms in $\partial_c(P_{xy})/\partial t$ are $O(T)$ and $O(St^{-2}T)$ respectively.

According to the above order of magnitude analysis, the quadratic part of the collisional source $P_{ii}$ is $O(St^{-2})$ smaller than the linear part. In addition, $\tilde{\omega}^{(2,22)}/\omega^{(2,2)} = 1/14 \ll 1$. Thus, the quadratic terms in $\partial_c(P_{xy})/\partial t$ and the $P_{kk}^2$ terms in $\partial_c(P_{ii})/\partial t$ are a factor of 350 smaller than the linear terms even for $St \sim 5$, which, as we shall see, is the smallest Stokes number for which the ignited state exists. Thus, we neglect these small terms and the collisional change of the stress tensor (3.7) reduces to

$$\left(\frac{\partial_c P_{jk}}{\partial t}\right)_i = -\frac{48\phi T^{3/2}}{5\pi^{1/2}}[(P_{jk} - p\delta_{jk}) + \tfrac{1}{21}\zeta_{jk} P_{xy}^2] \tag{3.14a}$$

with $$\zeta_{xx} = \zeta_{yy} = -\tfrac{1}{2}\zeta_{zz} = 1, \quad \zeta_{xy} = 0. \tag{3.14b}$$

Using (2.8) and substituting the collisional change of the stress tensor (3.14) into the

balance equations (2.7) for $P_{xx}$, $P_{yy}$, and $P_{zz}$, one obtains the stress tensor in terms of the temperature

$$P_{xx}-p=\left(2-\frac{72}{35}\frac{\omega}{St}\right)(1+\tfrac{24}{5}St\omega)^{-1}T, \tag{3.15}$$

$$P_{yy}-p=-\left(1+\frac{72}{35}\frac{\omega}{St}\right)(1+\tfrac{24}{5}St\omega)^{-1}T, \tag{3.16}$$

$$P_{zz}-p=-\left(1-\frac{144}{35}\frac{\omega}{St}\right)(1+\tfrac{24}{5}St\omega)^{-1}T, \tag{3.17}$$

$$P_{xy}=-\tfrac{12}{5}St\omega(1+\tfrac{24}{5}St\omega)^{-1}T. \tag{3.18}$$

Here $\omega=\phi T^{1/2}/\pi^{1/2}$. To complete the solution we need to determine $T$. This is accomplished by substituting (3.16) and (3.18) for $P_{yy}$ and $P_{xy}$ in the $xy$-component of (2.7) to yield a quartic equation for $T^{1/2}$:

$$\omega^2[4032St^2\omega^2+(1740St-140St^3)+175]=0 \tag{3.19}$$

which can be solved analytically. The three distinct roots are

$$T_1=0, \tag{3.20a}$$

$$T_2^{1/2}=\frac{5\pi^{1/2}}{144}\frac{St}{\phi}\left[\frac{(St^2-\frac{87}{7})-[(St^2-\frac{87}{7})^2-12^2]^{1/2}}{2St^2}\right], \tag{3.20b}$$

$$T_3^{1/2}=\frac{5\pi^{1/2}}{144}\frac{St}{\phi}\Theta(St), \tag{3.20c}$$

with

$$\Theta=\left[\frac{(St^2-\frac{87}{7})+[(St^2-\frac{87}{7})^2-12^2]^{1/2}}{2St^2}\right]\leqslant 1. \tag{3.20d}$$

$T_2$ is unstable because the shear work is larger than the viscous dissipation when $T>T_2$, and vice versa. $T_3\gg 1$ is stable and corresponds to the ignited state.

In addition to the solutions $T_2$ (unstable) and $T_3$ (ignited state), which we obtained by assuming that the velocity distribution function was a truncated Hermite expansion (3.6), we obtain a third solution, $T_1=0$, corresponding to a velocity distribution that is a delta-function, i.e. $f(C)=n\delta(C)$. Although this velocity distribution satisfies both the Boltzmann equation and the balance equation for the stress tensor, it has always been neglected in the standard kinetic theory for dilute gases. However, this solution is physically relevant to a dilute sheared gas–solid suspension and corresponds to the quenched state observed in the numerical simulations. Most of the particles in the quenched state travel with the velocity of the fluid, i.e. $C=0$. However, occasional shear-induced collisions occur and cause a small fraction of the particles to have substantial velocity fluctuations. Because we have neglected shear-induced collisions in this section, we are unable to determine the small (but non-zero) magnitude of the temperature in the quenched state at present, but we will address that problem in the following section.

Returning to our solution (3.15)–(3.18) and (3.20$c$) for the ignited state, the dimensional viscosity of the particle phase and the normal stress differences are

$$\mu_p=\Theta(St)\mu_p^* \quad\text{with}\quad \mu_p^*=\frac{5\pi^{1/2}}{48}\rho_p T^{1/2}a, \tag{3.21a,b}$$

and

$$\frac{P_{xx}-P_{yu}}{p}=\frac{18}{St^2\Theta+6}, \qquad \frac{P_{yy}-P_{zz}}{p}=-\frac{\frac{9}{7}}{St^2\Theta+6}. \tag{3.22a,b}$$

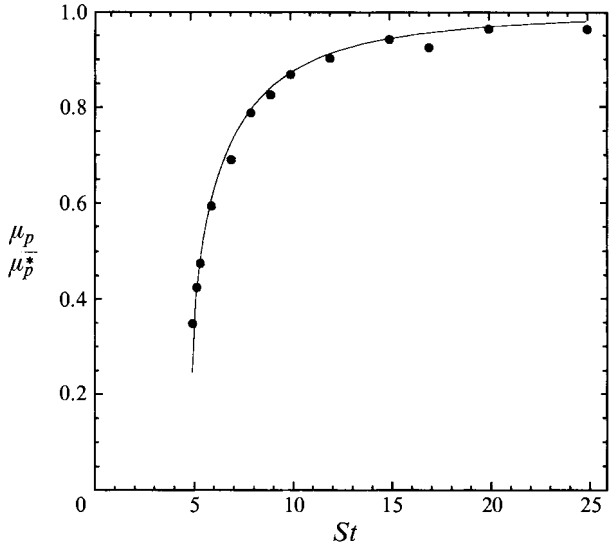


FIGURE 1. The effective viscosity of the particle phase is plotted as a function of $St$ of $\phi = 0.01$. The line corresponds to the theoretical prediction and the symbols to the simulation results.

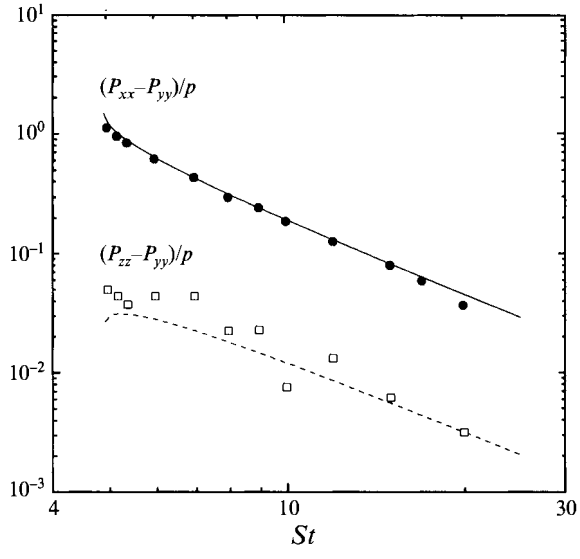


FIGURE 2. The normal stress differences are plotted as a function of $St$ for $\phi = 0.01$. The lines are theoretical predictions and the symbols are the simulation results.

Comparisons between results derived from the kinetic theory and data obtained from dynamic simulations are shown in figures 1 and 2 for particle viscosity and normal stress differences, respectively. The agreement is quite good even for Stokes numbers as small as 5 – the smallest value for which the ignited state was observed in the simulations. In the asymptotic limit $St \gg 1$, the viscosity reduces to $\mu_p^*$, which is identical to the viscosity of a dilute gas of hard spheres. This is not surprising because the behaviour of the particles will become like that of hard-sphere molecules as $St \to \infty$ in the sense that the particles travel in free flight without significant energy dissipation between successive collisions.

According to (3.22), the normal stresses satisfy

$$P_{xx} > P_{zz} > P_{yy}. \tag{3.23}$$

$P_{xx}$ is the largest normal stress because the streaming term only contributes to the $xx$-component of the pressure tensor. $P_{zz}$ is slightly larger than $P_{yy}$ because the coefficient in front of $P_{xy}^2$ in the $zz$- and $yy$-components of the collisional source (3.14) are slightly different, that is collisions convert the moment $P_{xy}$ into $P_{zz}$ more efficiently than they do into $P_{yy}$. In the asymptotic limit $St \gg 1$, the temperature and normal pressure reduce to

$$T^{1/2} = \frac{5\pi^{1/2}}{144}\frac{St}{\phi}\left[1 - \frac{87}{7}\frac{1}{St^2} + O\left(\frac{1}{St^4}\right)\right], \tag{3.24}$$

$$P_{xx} = \left(1 + \frac{81}{7}\frac{1}{St^2}\right)T, \quad P_{yy} = \left(1 - \frac{45}{7}\frac{1}{St^2}\right)T, \quad P_{zz} = \left(1 - \frac{36}{7}\frac{1}{St^2}\right)T. \tag{3.25}$$

Note that the temperature is inversely proportional to $\phi^2$ just as in a dilute granular flow of inelastic particles (Lun *et al.* 1984), even though the scalings of the dissipation due to inelastic collisions and viscous drag are different, i.e. $\phi^2 T^{3/2}$ and $\phi T$, respectively. Using (3.24), the first and second normal pressure differences are obtained:

$$\frac{P_{xx} - P_{yy}}{p} = \frac{18}{St^2} + O\left(\frac{1}{St^4}\right), \qquad \frac{P_{yy} - P_{zz}}{p} = -\frac{9}{7}\frac{1}{St^2} + O\left(\frac{1}{St^4}\right) \tag{3.26a,b}$$

As $St \to \infty$, $P_{xx} = P_{yy} = P_{zz}$ as in a Newtonian fluid. The results (3.25) and (3.26) should be compared with the corresponding expressions given by the Chapman–Enskog expansion up to Burnett order for hard spheres:

$$\frac{P_{xx} - P_{yy}}{P} = 2.028\frac{\mu_p^2\gamma^2}{P^2} = \frac{18.252}{St^2}, \tag{3.27}$$

$$\frac{P_{yy} - P_{zz}}{P} = -0.172\frac{\mu_p^2\gamma^2}{P^2} = -\frac{1.548}{St^2}. \tag{3.28}$$

Burnett (see Chapman & Cowling 1970, p. 289) solved the Boltzmann equation to obtain the velocity distribution using the Chapman–Enskog expansion which expands the velocity distribution in a series and his results are exact to $O(\gamma^2)$. There is only a small difference between the numerical coefficients in our and Burnett's results. This error is due to the assumed form of the distribution function in our analysis. The drag does not alter the normal stress differences to this order. The truncated Hermite expansion gives a very good approximation to the solution of the Boltzmann equation for the shear viscosity and normal stress differences of the particle phase and it avoids a tedious iteration procedure required in the Chapman–Enskog method. In addition, the Hermite expansion provides an accurate expression for the collisional change of the second moment. For $St \gg 1$, one has the same dimensional constitutive relation for the stress tensor as for a dilute molecular gas, i.e.

$$\boldsymbol{P} = \rho_s T\boldsymbol{I} - 2\mu_p\hat{\boldsymbol{D}}, \quad \hat{\boldsymbol{D}} \equiv \tfrac{1}{2}(\boldsymbol{\nabla}\langle\boldsymbol{v}\rangle + \boldsymbol{\nabla}\langle\boldsymbol{v}\rangle^T) - \tfrac{1}{3}\boldsymbol{I}\boldsymbol{\nabla}\cdot\langle\boldsymbol{v}\rangle. \tag{3.29}$$

From the above observations, we can also deduce the dimensional constitutive relations for the heat flux of the particle phase for $St \gg 1$ from dilute gas theory (Chapman & Cowling 1970, p. 168):

$$\boldsymbol{q} = -k_p^*\boldsymbol{\nabla}T \quad \text{with} \quad k_p^* = \frac{25\pi^{1/2}}{64}\rho_p T^{1/2}a. \tag{3.30a,b}$$

Although the expression for the particle viscosity in the limit $St \to \infty$ becomes the

same as that for a molecular gas, the suspension can be said to exhibit a shear-thickening behaviour. The granular temperature cannot be specified independent of the shear rate. It is controlled by the balance of shear work and dissipation due to drag and is proportional to $[(St/\phi)(\gamma a)]^2$ in the high Stokes number limit. Thus, the shear viscosity is proportional to shear rate squared at $St \to \infty$.

In order to obtain a real solution for the temperature in (3.20), one must satisfy the criterion that the expression within the square root is greater than zero, i.e.

$$(St^2 - \tfrac{87}{7})^2 - 12^2 \geqslant 0 \quad \text{or} \quad St \geqslant (\tfrac{171}{7})^{1/2}. \tag{3.31}$$

In other words, we must have $St$ at least as large as $St_c = (171/7)^{1/2}$ to obtain the ignited state in a dilute gas–solid suspension. Otherwise, the only solution is the quenched state.

Although the Stokes number based on shear rate is $O(1)$ as $St \to St_c$, the velocity variance in the ignited state remains quite large $T \to (0.075/\phi)^2$, so that $St_T \gg 1$ and hydrodynamic interactions may always be neglected in the ignited state of a dilute suspension. For Stokes numbers that are close to the critical value $St_c = (171/7)^{1/2}$, the deviation of the velocity distribution from an isotropic Maxwellian becomes large and the expressions for the viscosity and the normal stress differences differ from the expressions for a molecular gas. The deviation of the particle viscosity from the Newtonian viscosity $\mu_p^*$ is given by the factor $\Theta$ whose dependence on the shear rate is expressed in (3.20$d$). It is interesting to note that the ratio of the particle viscosity to the Newtonian value, i.e. $\Theta = \mu_p/\mu_p^*$, increases with increasing shear rate (shear thickening) whereas it decreases with increasing shear rate (shear thinning) in the molecular case (Zwanzig 1979). The molecular gas becomes more dissipative as the shear rate is increased and $\gamma a$ approaches $T^{1/2}$. However, the opposite is true for the particle suspension. The granular temperature is proportional to $\gamma^4$, so the ratio $\gamma a/T^{1/2}$ actually becomes smaller and the velocity distribution closer to Maxwellian as the shear rate increases.

Using a moment method based on a truncated Hermite expansion for the velocity distribution, two stable steady states have been obtained. The ignited and quenched states found in numerical simulations correspond respectively to $T_1$ and $T_3$. The result that the ignited state exists only for $St > (171/7)^{1/2}$ is consistent with the numerical simulations which show the ignited state for $St \geqslant 5$ (cf. figure 1). Because the ignited state can exist even for very small volume fractions, we may expect that for small enough $\phi$ both the ignited and quenched states are possible. In this region of multiple steady states, the unstable steady state $T_2$ may be expected to provide a boundary between the initial velocity variances that will lead to the ignited or quenched state. According to (3.20), this unstable solution is $T_2 = O(St^3\phi)^{-2}$.

It will be shown in the next section that shear-induced collisions lead to an $O(St^3\phi)$ temperature. If the Stokes number is increased to a critical value for which $St^3\phi = O(1)$, then the shear-induced variance will be as large as the unstable solution $T_2$ and we may expect that the system will be ignited independent of initial conditions. This hypothesis will be confirmed and a quantitative value of the critical Stokes number will be obtained in §5.

## 4. Quenched state ($\tau_c \gg \tau_v$)

Most of the collisions in the quenched state are shear induced. These collisions are infrequent and $\tau_c \gg \tau_v$. We expect the velocity distribution in this state to be very

different from the Maxwellian, because the particles relax close to the local fluid velocity between successive collisions and, at any time, the fraction of the particles that have velocities significantly different from the velocity of the fluid is small. Before calculating the stress tensor from the moment method, we will obtain a qualitative understanding of the velocity distribution function by examining the Boltzmann equation. The $O(\Delta f/\tau_c)$ collision term is small compared to the $O(\gamma f)$ streamline crossing and the $O(f/\tau_v)$ drag term in the limit $\phi \ll 1$ and $St \gg 1$ except near $C = 0$. By neglecting the collision term in the Boltzmann equation, one obtains a first-order linear partial differential equation. For simplicity, we can integrate the equation over $C_z$ to obtain

$$(StC_y + C_x)\frac{\partial f_{xy}}{\partial C_x} + C_y\frac{\partial f_{xy}}{\partial C_y} + 2f_{xy} = 0, \tag{4.1}$$

where

$$f_{xy}(C_x, C_y) = \int_{-\infty}^{\infty} \mathrm{d}C_z f.$$

This equation can be solved using the method of characteristics to give

$$f_{xy}[C_x(t), C_y(t)] = f_0\,\mathrm{e}^{2t}, \tag{4.2a}$$

$$C_x(t) = C_{x0}\,\mathrm{e}^{-t} - C_{y0}\,St\,t\,\mathrm{e}^{-t}, \quad C_y(t) = C_{y0}\,\mathrm{e}^{-t}. \tag{4.2b,c}$$

Here the characteristic variable $t$ can be thought of as the time following the collision. As $t \to \infty$, $C_x$ and $C_y \to 0$ and $f \to \infty$. The determination of $C_{x0}$, $C_{y0}$ and $f_0$ requires a complicated analysis of the shear-induced collisions, which we shall not pursue.

Integrating (4.1) over $C_x$, we obtain a first-order linear ordinary differential equation,

$$f_y + C_y\frac{\mathrm{d}f_y}{\mathrm{d}C_y} = 0, \tag{4.3}$$

where the marginal distribution function $f_y$ is a simple reduced distribution that retains the main physical features of $f$ and is defined as

$$f_y(C_y) = \int_{-\infty}^{\infty} \mathrm{d}C_x \int_{-\infty}^{\infty} \mathrm{d}C_z f(C). \tag{4.4}$$

The solution of (4.3) is

$$f_y = k_1/|C_y|, \tag{4.5}$$

where $k_1$ is a constant whose determination requires a detailed analysis of the sheared-induced collisions.

The above analysis shows that the velocity distribution has a highly peaked structure and is singular at $C = 0$. The fact that $\int \mathrm{d}C_y f_y$ gives a logarithmic singularity indicates that most of the particles are close to $C_y = 0$. The singularity would need to be removed by including shear-induced collisions. This result suggests that the majority of the particles travel with the velocity of the fluid. However, when a shear-induced collision occurs, each of the particles gains an $O(\gamma a)$ velocity on impact and travels an $O(Sta)$ distance in the $y$-direction. By crossing streamlines, the particle's fluctuating velocity in the $x$-direction grows to $O(St\gamma a)$.

The momentum transferred by particle translation will lead to an increase of the effective viscosity of the suspension. Since the rate at which the particle experiences shear-induced collisions is $O(\gamma a\phi)$ and the time that its fluctuating velocity persists is $\tau_v$, a small $O(St\phi)$ fraction of particles is not moving with the local fluid velocities at any given time. Therefore, we expect the order of magnitude of the components of the stress tensor for the particle phase to be $P_{yy} = O(St\phi)$, $P_{zz} = O(St\phi)$, $P_{xx} = O(St^3\phi)$,

and $P_{xy} = O(St^2\phi)$. Note that the first normal stress difference $P_{xx} - P_{yy}$ is very large in the quenched state.

Following the same steps that were applied to the ignited state, the stress tensor in the quenched state can be obtained as a solution of the balance equation for the stress tensor (2.7) with (2.12). In order to evaluate the collisional change in the stress tensor due to shear-induced collisions, an appropriate velocity distribution function must be assumed. Although particles with $O(St\gamma a)$ velocities might undergo a second, variance-driven collision after a shear-induced collision, the probability of such a collision is small, $O(St^2\phi)$. Therefore, we can obtain the leading-order collisional change of the stress tensor by assuming that the velocities of the colliding particles are equal to the local fluid velocity, i.e. $f(\boldsymbol{C}) = n\delta(\boldsymbol{C})$.

By assuming that the velocity distribution function is a delta-function, we have $\boldsymbol{w} = 0$ and $\boldsymbol{g} = \Delta\boldsymbol{u}$. Using (2.17), the shear-induced collisional change of the stress tensor is given by

$$\left(\frac{\partial_c P_{ij}}{\partial t}\right)_q = \frac{3}{\pi}\int_{\Delta\boldsymbol{u}\cdot\boldsymbol{k}>0} (\Delta\boldsymbol{u}\cdot\boldsymbol{k})^3 k_i k_j \,\mathrm{d}\boldsymbol{k} \tag{4.6}$$

with

$$(\Delta\boldsymbol{u}\cdot\boldsymbol{k}) = -2k_x k_y, \tag{4.7}$$

where the subscript $q$ indicates that this estimate of the collision integral is accurate for the quenched state. After integration, one obtains

$$\left(\frac{\partial_c P_{xx}}{\partial t}\right)_q = \left(\frac{\partial_c P_{yy}}{\partial t}\right)_q = 4\left(\frac{\partial_c P_{zz}}{\partial t}\right)_q = \frac{256}{315\pi}\phi \tag{4.8}$$

and

$$\left(\frac{\partial_c P_{xy}}{\partial t}\right)_q = -\frac{8}{35}\phi. \tag{4.9}$$

Although energy is conserved in each collision, there is a shear-induced collisional source of particle temperature associated with the transformation of the energy of the mean motion into fluctuations:

$$P_{xy} + \frac{\langle C^2\rangle}{St} = \left(\frac{\partial_c C^2}{\partial t}\right)_q = \frac{576}{315\pi}\phi > 0. \tag{4.10}$$

The shear-induced collisional source can be neglected when $\langle C^2\rangle^{1/2} \gg \gamma a$ as it is in the ignited state.

Substituting for $\partial_c(P_{ij})/\partial t$ in the balance equation (2.7) from (4.8) and (4.9) and solving for the stress tensor of the particle phase yields

$$P_{xx} = \frac{64}{315\pi} St^3\phi\left[1 + \frac{9\pi}{16}\frac{1}{St} + \frac{2}{St^2}\right], \tag{4.11a}$$

$$P_{yy} = 4P_{zz} = \frac{128}{315} St\phi, \tag{4.11b}$$

$$P_{xy} = -\frac{64}{315\pi} St^2\phi\left[1 + \frac{9\pi}{16}\frac{1}{St}\right], \tag{4.11c}$$

Whereas the stress in the particle phase was larger than that in the gas phase when the suspension was ignited, the particle phase makes a small $O(St^3\phi^2)$ contribution to the stress tensor of the suspension in the quenched state. Consequently, the stress tensor of the quenched suspension is dominated by the gas phase.

Neglecting the effects of particle–particle collisions, the effective viscosity of a suspension of particles with $C = 0$ in simple shear flow can be described by the Einstein relation (Einstein 1906):

$$\mu_{eff} = \mu[1 + \tfrac{5}{2}\phi + O(\phi^2)]. \tag{4.12}$$

In the quenched state, the effective viscosity will be enhanced by the momentum transferred due to the random flight of particles after shear-induced collisions. By summing up contributions from (4.11*c*) and (4.12), the effective viscosity is given by

$$\mu_{eff} = \mu[1 + \tfrac{5}{2}\phi + ((32/35\pi)\, St^3 + \tfrac{18}{35} St^2)\, \phi^2 + O(\phi^2)]. \tag{4.13}$$

Simple additivity is justified since the Einstein term comes from the many particles following the local fluid velocity and the kinetic term from the few that recently collided. Since the criterion for the existence of the quenched state is $St^3\phi \leqslant O(1)$, the contribution from shear-induced collisions will not exceed that from the $O(\phi)$ term.

Hydrodynamic particle interactions have been neglected in the preceding analysis. This approximation is valid even in the quenched state as long as $St \gg 1$.

We have been able to calculate the leading-order behaviour of the stress tensor for $St^3\phi \ll 1$ by perturbing from a state in which the velocities of the colliding particles are equal to the local fluid velocities. However, we are interested in the behaviour of the quenched state for concentrations up to the critical point, $St^3\phi \sim O(1)$. To test the accuracy of the preceding approximate analysis and obtain accurate results for $St^3\phi \sim O(1)$, we will conduct Monte Carlo simulations which solve the full nonlinear Boltzmann equation. As discussed at length by Bird (1970) and Hopkins & Shen (1992), the Monte Carlo technique has been devised to mimic the dynamics described by the Boltzmann equation. Since the details of the method can be found in Bird (1970) and Hopkins & Shen (1992), we only review the key points and indicate the minor modifications needed to include the effects of viscous drag and shear-induced collisions.

The key ideas of the direct-simulation Monte Carlo method (DSMC) are: (*a*) the uncoupling of particle translations and collisions during the time step $\Delta t$, and (*b*) the simulation of particle collisions without keeping track of position coordinates between successive collisions. An impact parameter is generated randomly before each collision and gives the local fluid velocity difference $\Delta \boldsymbol{u}$ needed to evaluate the rate of shear-induced collisions. Idea (*a*) is valid provided that the condition $\Delta t \ll \min(\tau_c, \tau_v)$ is satisfied. Idea (*b*) is valid provided that the system is so small or homogeneous that the spatial variations are negligible.

The simulation procedure during the time step $\Delta t$ is described as follows. A collisional configuration $(\boldsymbol{v}_1, \boldsymbol{v}_2, \boldsymbol{k})$ is created by choosing at random the fluctuation velocities $\boldsymbol{C}_1$ and $\boldsymbol{C}_2$ from the set of velocities of the simulated particles and a direction $\boldsymbol{k}$ from a uniform distribution in space. The particle velocities $\boldsymbol{v}_1$ and $\boldsymbol{v}_2$ relative to the mean velocity at the point of contact are obtained by adding a mean velocity component to the chosen fluctuating velocities $\boldsymbol{C}_1$ and $\boldsymbol{C}_2$:

$$\boldsymbol{v}_1 = \boldsymbol{C}_1 + k_y \boldsymbol{e}_x, \quad \boldsymbol{v}_2 = \boldsymbol{C}_2 - k_y \boldsymbol{e}_x. \tag{4.14}$$

A collision is impending if $\boldsymbol{g}\cdot\boldsymbol{k} > 0$. With the assumption of molecular chaos, the fraction of colliding particles with $\boldsymbol{C}_1$ in $\mathrm{d}\boldsymbol{C}_1$, $\boldsymbol{C}_2$ in $\mathrm{d}\boldsymbol{C}_2$ and $\boldsymbol{k}$ in $\mathrm{d}\boldsymbol{k}$ in the set of all collisional configurations is represented by $p(\boldsymbol{C}_1, \boldsymbol{C}_2, \boldsymbol{k})\, \mathrm{d}\boldsymbol{k}\, \mathrm{d}\boldsymbol{C}_1\, \mathrm{d}\boldsymbol{C}_2$, where

$$p(\boldsymbol{C}_1, \boldsymbol{C}_2, \boldsymbol{k}) = \frac{nN\hat{f}(\boldsymbol{C}_1)\hat{f}(\boldsymbol{C}_2)\, \sigma^2(\boldsymbol{g}\cdot\boldsymbol{k})}{2v}. \tag{4.15}$$

Here $\hat{f}$ is the normalized distribution $f/n$ and $\upsilon$ is the total dimensional collision frequency in the simulated system given by

$$\upsilon = \frac{nN}{2}\int \hat{f}(\boldsymbol{C}_1)\hat{f}(\boldsymbol{C}_2)\,\sigma^2(\boldsymbol{g}\cdot\boldsymbol{k})\,\mathrm{d}\boldsymbol{k}\,\mathrm{d}\boldsymbol{C}_1\,\mathrm{d}\boldsymbol{C}_2. \tag{4.16}$$

The samples chosen at random must be weighted according to $\boldsymbol{g}\cdot\boldsymbol{k}$ to form the configuration distribution defined in (4.15). In practice, the standard acceptance–rejection method is adopted by determining the effective maximum value $\zeta \equiv |\boldsymbol{g}\cdot\boldsymbol{k}|_{max}$ for the $N$ particles in the simulated system. If a random number $R$ uniformly distributed between 0 and 1 satisfies

$$R < (\boldsymbol{g}\cdot\boldsymbol{k})/\zeta \tag{4.17}$$

then the pair is accepted as a collision pair. Clearly, $\zeta$ is a positive number and both accuracy and computation time increase with increasing $\zeta$. In the limit $\zeta\to\infty$, the criterion is exact. If the pair is accepted for a collision, the post-collision velocity components are calculated.

Between collisions the fluctuating velocity of a particle changes due to both streamline crossing and viscous drag according to

$$\frac{\mathrm{d}\boldsymbol{C}}{\mathrm{d}t} = -\frac{1}{St}\boldsymbol{C} - \boldsymbol{C}\cdot\nabla\boldsymbol{u}, \tag{4.18}$$

which can be solved to give

$$\boldsymbol{C}(t+\Delta t) = \boldsymbol{C}(t)\,\mathrm{e}^{-\Delta t/St} - C_y(t)\,\Delta t\,\mathrm{e}^{-\Delta t/St}\,\boldsymbol{e}_x. \tag{4.19}$$

Thus, after each collision described above, the fluctuating velocity of every particle in the simulated system will change as given in (4.18). After each time interval $\Delta t$, a collision will take place. The collision time interval $\Delta t$ is chosen as the reciprocal of the average dimensional frequency of collision $\upsilon$. This can be calculated using the numerical equivalent of (4.16):

$$\Delta t = 1/\upsilon = (\tfrac{1}{2}Nn\pi\sigma^2\langle \boldsymbol{g}\cdot\boldsymbol{k}\rangle)^{-1}, \tag{4.20}$$

where $\langle\cdot\rangle$ denotes an average over all collisions. Finally, the procedure is repeated until the system reaches steady state.

When the velocities of the colliding particles are equal to the local fluid velocities at their centres, the average dimensional $\tau_c$ can be evaluated using (4.16):

$$\tau_c = N/\upsilon = \tfrac{1}{2}\pi(\gamma\phi)^{-1} \gg \tau_v. \tag{4.21}$$

This result provides an asymptotic value of $\tau_c$ for $St^3\phi \ll 1$ and will be used as a consistency check for the simulation. Since shear-induced collisions dominate in the quenched state, a large number of particles is required in the simulation. For example, if we consider a simulated system with $\phi = 5\times10^{-4}$ and $St \sim O(10)$, we have

$$\tau_v = St \sim O(10), \quad \tau_c \sim \pi/2\phi \sim 3\times10^3$$

and

$$\Delta t \sim \tau_c/N \sim (10^3/N).$$

If we choose $\Delta t \sim O(1)$ to satisfy the criterion $\Delta t \ll \min(\tau_c, \tau_v)$, then we must have $O(10^3)$ particles in the system.

The results of Monte Carlo simulations are shown in figures 3–6. The variation of

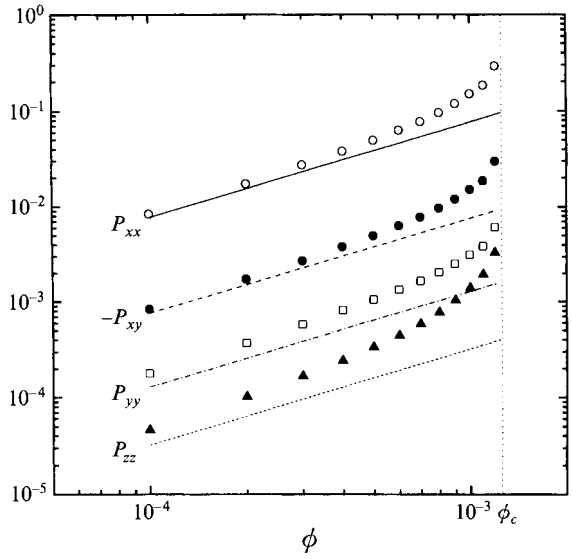


FIGURE 3. The variation of the stress tensor with the volume fraction for $St = 10$. The lines correspond to the asymptotic analysis and the symbols to the simulation results.

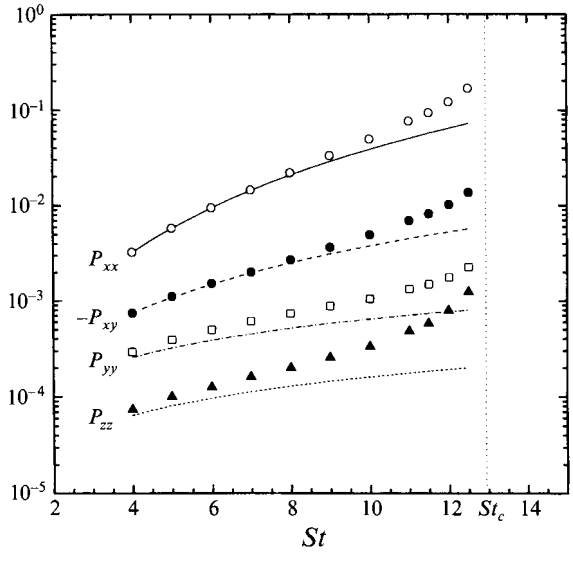


FIGURE 4. The variation of the components of the stress tensor with Stokes number for $\phi = 5 \times 10^{-4}$. The lines correspond to the asymptotic analysis and the symbols to the simulation results.

the stress tensor with volume fraction is shown in figure 3 for $St = 10$ along with the asymptotes (4.11) obtained from the moment method. As $\phi$ increases, the deviation from the asymptotic curve grows owing to the increasing frequency of variance-driven collisions. The simulation points in figure 3 extend up to $\phi_c = 1.4 \times 10^{-3}$. When $\phi \geqslant \phi_c(St)$, the system is ignited, even when the initial variance is zero. Figure 4 shows the variation of the stress tensor with $St$ for $\phi = 5 \times 10^{-4}$. The deviations from the asymptotic curves increase as $St$ increases and finally the system attains the ignited

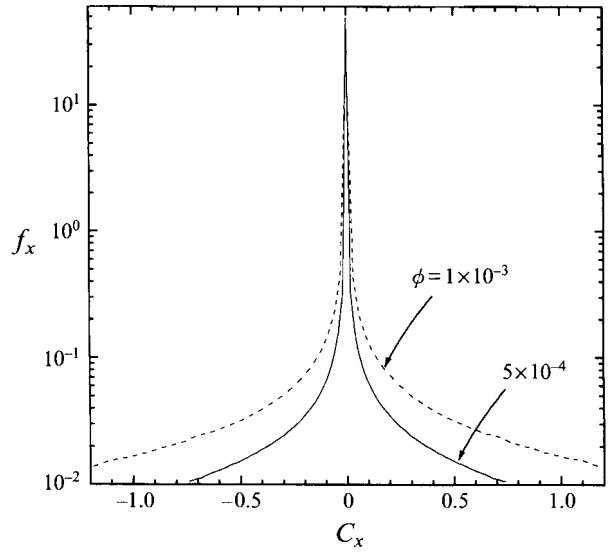


FIGURE 5. The marginal velocity distribution function $f_x(C_x)$ for $\phi = 5\times10^{-4}$ and $1\times10^{-3}$.

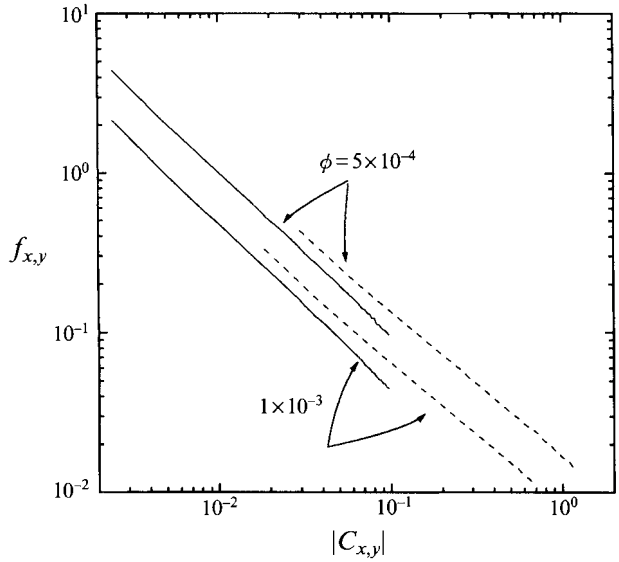


FIGURE 6. Log–log plots of the marginal velocity distribution functions $f_x$ and $f_y$ for $\phi = 5\times10^{-4}$ and $1\times10^{-3}$. The solid lines correspond to $f_y(C_y)$ and the dashed lines to $f_x(C_x)$.

state when $St$ is larger than a critical Stokes number of about 13. All the simulation data were obtained with an initial condition of zero velocity variance.

The knowledge of the velocity of all the particles allows one, in principle, to construct the velocity distribution function from the simulation. However, this is a complicated function to represent, since it depends on all three velocity components. Consequently, we will focus on the marginal distribution functions $f_x$ and $f_y$. Here $f_x$ has a definition analogous to (4.4) for $f_y$. The marginal velocity distribution $f_x$ obtained from the simulation is shown in figure 5 for $St = 10$ and $\phi = 5\times10^{-4}$ and $1\times10^{-3}$. When a shear-induced collision occurs, the particle has an $O(St\gamma a)$ velocity for an $O(\tau_v)$

time period and then relaxes to an $O(\gamma a)$ velocity after an $O[\ln(St)\,\tau_v]$ time. Therefore, there is an $O(1)$ fraction of the particles with fluctuation velocities much smaller than $O(\gamma a)$, an $O[St\phi \ln(St)]$ fraction with $O(\gamma a)$ velocities, and an $O(St\phi)$ fraction with $O(St\gamma a)$ velocities. The velocity distributions in figure 5 have highly peaked structures. Note that figure 5 is a logarithm–linear plot, so the distribution is even more peaked than it appears. As expected, the velocity distribution for the higher concentration has a higher fraction of particles with velocities different from local fluid velocity. Figure 6 shows log–log plots of $f_x$ and $f_y$. They are nearly linear, indicating that $f_x$ and $f_y$ are given approximately by power laws, $f_x \propto C_x^{-0.91}$ and $f_y \propto C_y^{-1.03}$. The scaling of $f_y$ is close to the result (4.5) obtained by analysing the Boltzmann equation. The power law for $f_x$ suggests that it differs from $1/C_x$ by a logarithmic factor, as might be expected from (4.2).

## 5. Transition from the quenched to ignited state

In the quenched state, the particle temperature grows as $St$ or $\phi$ increases toward the critical point. Beyond this point, the system jumps to the ignited state. A simple explanation for the existence of the critical $St$ for a fixed $\phi$ or the critical $\phi$ for a fixed $St$ is as follows. If the shear-induced variance is greater than the variance of the unstable state $T_2$, then the imposed shear will create enough velocity fluctuations to take the suspension past the unstable state even when the initial variance is zero. Consequently, only the ignited state will exist beyond the critical point. According to this simple argument, the critical point can be estimated as the point where the $O(St^3\phi)$ shear-induced temperature is as large as the $O(St^3\phi)^{-2}$ unstable temperature. Thus, the critical point is $St^3\phi \sim O(1)$. Through simulations the critical point can be determined and an $St_c$–$\phi_c$ diagram can be constructed. However, a theoretical prediction is also desirable. A quantitatively accurate prediction would require the determination of the full velocity distribution function from the Boltzmann equation near the critical point where it is neither close to the Maxwellian nor to a delta-function. However, a modified moment method, which takes into account the effects of both variance-driven and shear-induced collisions, will explain qualitatively the multiple steady states and hysteresis found in the simulation.

The stress tensor in the quenched state resulting from the shear-induced collisions alone is quite close to the results from simulation as shown in figures 3 and 4. However, near the critical point, the exclusive consideration of shear-induced collisions will lead to an underestimation of the temperature owing to the increasing possibility of a second collision after a shear-induced collision. Because the majority of the particles have fluctuating velocities that are either very large or very small compared to $\gamma a$, we can superimpose the contributions of the variance-driven and shear-induced collisions additively:

$$\frac{\partial_c P_{ij}}{\partial t} = \left(\frac{\partial_c P_{ij}}{\partial t}\right)_i + \left(\frac{\partial_c P_{ij}}{\partial t}\right)_q. \tag{5.1}$$

In §3, we kept the contribution of $P_{xy}^2$ in the collisional change of the stress tensor due to variance-driven collisions. However, the primary effect of the $P_{xy}^2$ term is just to give the slight difference between $P_{yy}$ and $P_{zz}$. For simplicity, we now neglect this nonlinear term, so that (3.15$a$) can be reduced to

$$\left(\frac{\partial_c P_{ij}}{\partial t}\right)_i = -\frac{48\phi T^{3/2}}{5\pi^{1/2}}(P_{ij} - p\delta_{ij}). \tag{5.2}$$

Substituting the change in the stress tensor due to both variance-driven and shear-induced collisions into the balance equation (2.7), the stress tensor can be expressed in terms of the temperature as

$$P_{xx} = \left[\frac{\eta T^{1/2} St\phi}{\Lambda} + \frac{\eta T^{1/2} St^3\phi}{\Lambda^3}\right] T + \left[\frac{(64/315\pi)\, St^3\phi}{\Lambda^3} + \frac{\frac{4}{35} St^2\phi}{\Lambda^2} + \frac{(128/315\pi)\, St\phi}{\Lambda}\right], \tag{5.3a}$$

$$P_{yy} = \left[\frac{\eta T^{1/2} St\phi}{\Lambda}\right] T + \left[\frac{(128/315\pi)\, St\phi}{\Lambda}\right], \tag{5.3b}$$

$$P_{zz} = \left[\frac{\eta T^{1/2} St\phi}{\Lambda}\right] T + \left[\frac{(32/315\pi)\, St\phi}{\Lambda}\right], \tag{5.3c}$$

$$-P_{xy} = \left[\frac{\eta T^{1/2} St^2\phi}{2\Lambda^2}\right] T + \left[\frac{(64/315\pi)\, St^2\phi}{\Lambda^2} + \frac{\frac{4}{35} St\phi}{\Lambda}\right], \tag{5.3d}$$

where $\eta = 24/5\,\pi^{1/2}$ and $\Lambda$ is defined as

$$\Lambda = 1 + \eta T^{1/2} St\phi. \tag{5.4}$$

The variance-driven and shear-induced collisions contribute to the first and second terms in the stress tensor, respectively. In the ignited state, $T \sim O(St/\phi)^2$ and the first term dominates. In the quenched state, $T \sim O(St^3\phi)$ and the second term is the dominant one.

The temperature of the system is determined by the energy balance (4.10) with (5.3*d*) for $P_{xy}$. Rearranging the energy equation, one obtains a quartic equation for $T^{1/2}$:

$$g(\xi) = a\xi^4 + b\xi^3 + c\xi^2 + d\xi + e = 0, \tag{5.5}$$

where $\xi = T^{1/2}$ and the coefficients are

$$a = -6\eta^2 St^2\phi^2, \quad b = \eta(St^3\phi - 12 St\phi), \quad c = \frac{576}{315\pi}\eta^2 St^3\phi^3 - 6, \tag{5.6a–c}$$

$$d = 2\eta\left(\frac{576}{315\pi} St^2\phi^2 + \frac{4}{35} St^3\phi^2\right), \quad e = \frac{128}{315\pi} St^3\phi + \frac{8}{35} St^2\phi + \frac{576}{315\pi} St\phi. \tag{5.6d, e}$$

The physically significant results correspond to positive real roots of (5.5). One root of (5.5) is always real and negative and will not be discussed here. To obtain a qualitative understanding of the other solutions, let us consider an asymptotic limit for which the solutions can be expressed analytically. In the limit $\phi \ll 1$, $St \gg 1$, and $St^3\phi \ll 1$, three positive real roots are obtained as follows:

(i) For $\xi \sim O(St^3\phi)^{1/2}$, (5.5) reduces to

$$c\xi^2 + e = 0. \tag{5.7}$$

As a result,

$$T_1 = \xi_1^2 = -\frac{e}{c} \cong \frac{1}{3}\left(\frac{64}{315\pi} St^3\phi\right). \tag{5.8}$$

This result corresponds to the temperature of the quenched state.

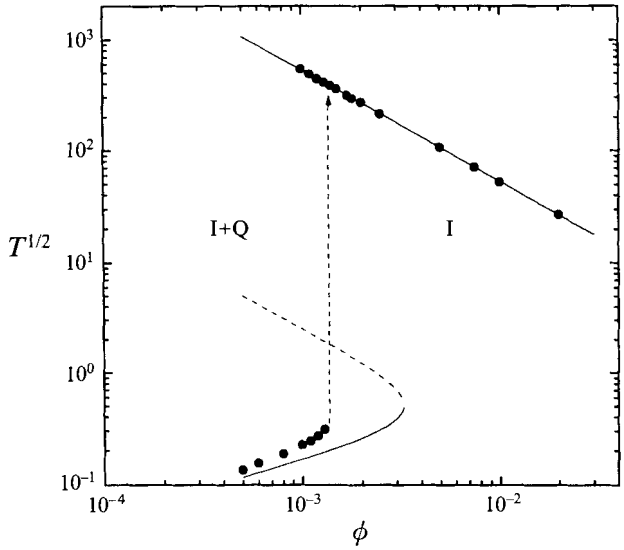


FIGURE 7. The granular temperature is plotted as a function of the volume fraction for $St = 10$. I and Q denote the ignited and quenched states, respectively. I + Q represents the region of multiple steady states.

(ii) For $\xi \sim O(St^3\phi)^{-1}$, (5.5) reduces to

$$b\xi^3 + c\xi^2 = 0, \tag{5.9}$$

As a consequence,

$$T_2^{1/2} = \xi_2 = -\frac{c}{b} = \frac{5\pi^{1/2}}{4}\frac{1}{St^3\phi}. \tag{5.10}$$

This solution is the unstable state.

(iii) For $\xi \sim O(St/\phi)$, (5.5) reduces to

$$a\xi^4 + b\xi^3 = 0. \tag{5.11}$$

Thus, we obtain the ignited state

$$T_3^{1/2} = \xi_3 = -\frac{b}{a} = \frac{5\pi^{1/2}}{144}\frac{St}{\phi}. \tag{5.12}$$

For $St \sim O(1)$, we have to solve (5.5) numerically. The roots of $g(\xi)$ depend on $St$ and $\phi$ and the numerical solutions are shown in figure 7 for $St = 10$ and in figure 8 for $\phi = 5 \times 10^{-4}$. For a given $St$ as shown in figure 7, we can have three different situations:

(i) four real roots (one negative and three positive: $T_1, T_2, T_3$), for $\phi < \phi_c$;

(ii) four real roots (one negative, one double root $T_1 = T_2$ and $T_3$), for $\phi = \phi_c$;

(iii) two real roots (one negative and one positive $T_3$), for $\phi > \phi_c$.

Obviously, only the positive roots are physically realizable since $\xi$ corresponds to particle velocity variance. For case (i), there are three positive roots: $T_1 < T_2 < T_3$. Two of them ($T_1$ and $T_3$) are stable and $T_2$ is unstable. In this case, one has multiple steady states: quenched and ignited states. If the initial velocity variance is larger than $T_2$, the particle temperature will evolve toward the ignited state. Otherwise, it will go to the quenched state. Since $T_2$ is proportional to $\phi^{-2}$, a very large initial variance is needed to achieve the ignited state for a very dilute system. Case (ii), $T_1 = T_2$, corresponds to the limit point in the lower solution branch where the stable quenched solution meets

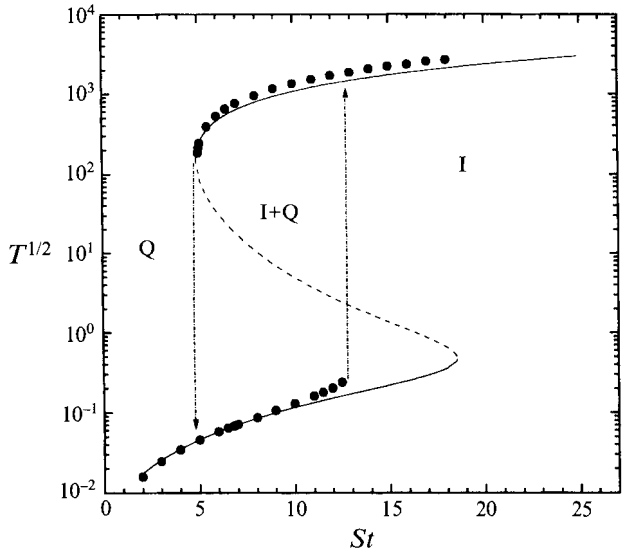


FIGURE 8. The granular temperature is plotted as a function of Stokes number of $\phi = 5 \times 10^{-4}$.

the unstable solution. It represents the critical point beyond which the quenched state no longer exists. For case (iii), only the ignited state exists. Beyond the critical point ($\phi_c$), the velocity variance due to shear-induced collisions is large enough to give ignition even if the system starts from zero variance.

The effect of the interstitial gas on the low-density asymptote occurring in granular flow theory can be examined using figure 7. Unlike the granular flow theory which neglects the fluid–particle interactions, we have multiple steady states for $\phi < \phi_c$. In the ignited state, the temperature diverges as $\phi \to 0$ because the rate of viscous dissipation is proportional to $\phi$ while the work done by the shear is independent of $\phi$. However, to attain the ignited state, the initial velocity variance of the system must be greater than $O(St^3\phi)^{-2}$, which becomes large as $\phi \to 0$. Thus, for a finite initial variance, the final state of the system will be quenched. In addition, when the temperature increases sufficiently, the Stokes drag law is no longer valid and nonlinear drag will play an important role in determining the temperature. The effects of nonlinear drag on the low-density asymptote will be discussed in the next session.

For a given $\phi$ the temperature of the system goes through three stages with increasing $St$. These stages are shown in figure 8. Below the critical point ($St_{c1}$) only the quenched state exists because the viscous drag is so large that the shear work is unable to sustain the ignited state. As $St$ is increased to the regime $St_{c1} < St < St_{c2}$, there are three roots $T_1 < T_2 < T_3$ corresponding to quenched, unstable and ignited states, respectively. The effects of increasing the Stokes number are to increase the viscous relaxation time of the particle and the probability of a second, variance-induced collision after an initial shear-induced collision. When $St = St_{c2}$, $T_2 = T_1$, corresponding to the critical point beyond which the quenched system will spontaneously jump to the ignited state. Beyond the critical point ($St_{c2}$), only the ignited state exists.

As shown in figure 8, hysteresis is observed when we vary $St$. If the system is in the quenched state for a given $\phi$ and one increases $St$ gradually, then the critical point where the system jumps to the ignited state is $St_{c2}(\phi)$. If $St$ is decreased gradually for a system in the ignited state, the critical point where the system jumps down to the quenched state is $St_{c1}$. Therefore, one may have either the ignited or quenched state for

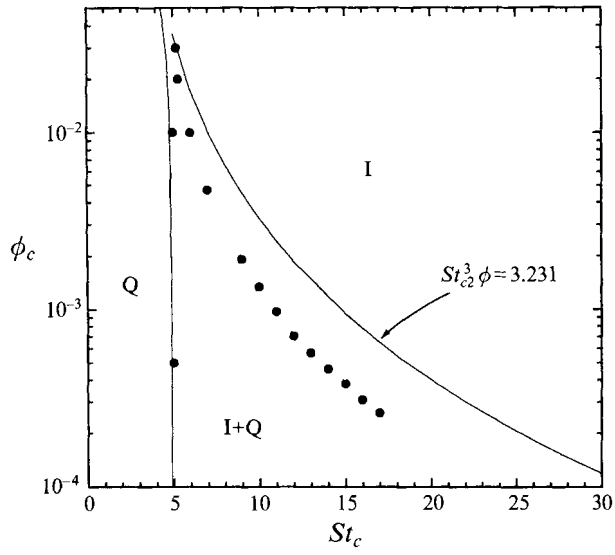


FIGURE 9. The critical Stokes numbers and volume fractions. The lines correspond to the theoretical predictions and the symbols to the simulation results.

$St_{c1} < St < St_{c2}$ depending on the previous history of the shear rate experienced by the suspension.

Now we will obtain the critical points $\phi_c$, $St_{c1}$, and $St_{c2}$ from the energy balance (5.5). The critical points occur when we have double roots. As a result, the critical temperature satisfies both $g(\xi_c) = 0$ and $g'(\xi_c) = 0$. Here $g'$ is the derivative of $g$ with respect to $\xi$, i.e.

$$g'(\xi_c) = 4a\xi_c^3 + 3b\xi_c^2 + 2c\xi_c + d = 0. \tag{5.13}$$

By solving (5.5) and (5.13) simultaneously for a given $\phi$, one obtains the $\xi_c(St_c, \phi_c)$ and $St_c(\phi_c)$. A $St_c$–$\phi_c$ diagram can be constructed from the numerical results and is shown in figure 9. To obtain analytical results, $g(\xi_c) = 0$ and $g'(\xi_c) = 0$ can also be solved for $St \gg 1$ as follows.

(i) When the double root is $T_2 = T_3$, the root is much larger than one for $\phi \ll 1$. Thus,

$$g(\xi_c) \approx a\xi_c^4 + b\xi_c^3 + c\xi_c^2 = 0 \tag{5.14}$$

and

$$g'(\xi_c) \approx 4a\xi_c^3 + 3b\xi_c^2 + 2c\xi_c = 0. \tag{5.15}$$

From (5.14) and (5.15) one has

$$\xi_c = -\frac{b}{2a} = \frac{5\pi^{1/2}}{288}\left(\frac{St}{\phi} - \frac{12}{St\phi}\right). \tag{5.16}$$

Substituting (5.16) for $\xi_c$ into (5.14) yields the condition $b^2 - 4ac = 0$. Thus the critical point is given as

$$St_{c1} = \sqrt{24}. \tag{5.17}$$

This result is independent of volume fraction and very close to the result $(171/7)^{1/2}$ obtained in §3. The small difference comes from the contribution of the nonlinear term to the collisional change of the stress tensor. It should be noted that $St_{c1}$ eventually decreases in a non-dilute suspension owing to the effect of the collisional stresses (Sangani *et al.* 1995) and the first stages of this behaviour can be seen in figure 9.

(ii) When the double root is $T_1 = T_2$, this root is $O(1)$ and neglecting terms of $O(St^3\phi^2)$ one obtains

$$g(\xi_c) \approx b\xi_c^3 + c\xi_c^2 + e = 0 \tag{5.18}$$

and

$$g'(\xi_c) \approx 3b\xi_c^2 + 2c\xi_c = 0. \tag{5.19}$$

From (5.18) one obtains

$$\xi_c = -\frac{2c}{3b} = \frac{5\pi^{1/2}}{6}\frac{1}{St^3\phi}. \tag{5.20}$$

Substituting (5.19) for $\xi_c$ into (5.19), the final result is

$$St_{c2}^3\,\phi_c = \left(\frac{7875\pi^2}{2304}\right)^{1/3} \approx 3.23. \tag{5.21}$$

By repeating calculations similar to those used to produce figures 7 and 8 for various values of $St$ and $\phi$, we are able to locate the critical points for different $St$ and $\phi$ from the simulations. These critical points constitute a $St_c$–$\phi_c$ diagram and are plotted in figure 9. The comparison between the theoretical analysis and simulation results is reasonably good. The lower critical point $St_{c1} \approx 5$ obtained by simulation is in good agreement with the theoretical results (5.17) because at this point the deviation from Maxwellian is moderate (though not asymptotically small) and can be described by the Hermite expansion. From simulations, the upper critical point is $St_c{}^3\phi_c \approx 1.5$. The value of the constant is smaller than the theoretical result 3.231 because of the underestimation of the collisional change in the stress tensor in the quenched state. We modelled the second collisions assuming that the velocity distribution could be described by the Hermite expansion. In the quenched state, we have $P_{xx} \gg P_{yy}$ and a highly peaked velocity distribution which is so far away from the Maxwellian that one cannot obtain quantitatively accurate results from the perturbed Maxwellian.

## 6. Suspension of particles with nonlinear drag

The viscous drag acting on most of the particles in the suspension can be described by Stokes law in the limit $Re_T \ll 1$. The Reynolds number in an ignited dilute suspension is small if $\rho_p/\rho_f \gg O(St^2/\phi)$. However, for a system with a fixed density ratio, the linear drag law cannot be valid as $St_T = St^2/\phi$ is increased indefinitely. Thus, nonlinear drag will always become important in the ignited state, if we decrease $\phi$ sufficiently.

In this section, we examine the effect of a nonlinear quasi-steady drag force on the dynamics of the suspension. In general, the drag depends on the time history of the particle velocity. However, for $Re_T \sim O(1)$, the history term decays rapidly for times larger than $O(a/\langle C^2\rangle^{1/2})$ (Lawrence & Mei 1995). The mean free time between collisions is $O(a\phi^{-1}/\langle C^2\rangle^{1/2})$ and so the particle experiences a steady drag for most of its flight. Therefore, we assume that the acceleration of the particles due to the drag force is of the form

$$\dot{\boldsymbol{v}} = -\frac{f_D}{\tau_v}(\boldsymbol{v}-\boldsymbol{u}), \tag{6.1}$$

where $f_D$ is the ratio of the drag to the Stokes drag. The drag coefficient is well represented for particle Reynolds numbers less than 1000 by (Clift, Grace & Weber 1978)

$$f_D = 1 + 0.15Re_p^{2/3}, \tag{6.2}$$

where $Re_p = 2\rho_f|\boldsymbol{C}|a/\mu$.

The velocity distribution function is given by the Boltzmann equation (2.3) with the acceleration of the particle due to the external force, $\dot{v}$, described by (6.1) and (6.2). The nonlinearity of the drag in addition to the nonlinearity of the collisional integral makes the problem difficult to approximate analytically. If $St$ is sufficiently large and $\gamma\tau_c$ sufficiently small, then collisions are frequent and they drive the velocity distribution toward the Maxwellian. Thus, it is possible to construct an approximate distribution function such as (3.6). However, if $\gamma\tau_c$ is large, the velocity distribution is far away from the Maxwellian and it is only possible to obtain solutions by computer simulation. Firstly, the moment method will be used to study a dilute suspension with nonlinear drag by assuming the velocity distribution to be a perturbation from the Maxwellian. Then, Monte Carlo simulations will be performed to solve the Boltzmann equation exactly and the results will be compared to those of the kinetic theory. For $St = 10$, the perturbation from the Maxwellian is found to be valid for volume fractions $\phi \geqslant 10^{-3}$ for which $\gamma\tau_c \leqslant 4$.

Following the moment method introduced in §2, taking $\Psi$ in (2.6) to be $\rho_s CC$, and using the dimensionless quantities defined in (3.13), one obtains the balance equation for the stress tensor:

$$(P_{jy}\delta_{ix} + P_{iy}\delta_{jx}) + \frac{2}{St}\langle f_D P_{ij}\rangle = \frac{\partial_c(P_{ij})}{\partial t}. \tag{6.3}$$

The viscous relaxation of the stress tensor due to the nonlinear drag is a nonlinear function of $P_{ij}$. Thus, the viscous relaxation of $P_{ij}$ must now be calculated using the assumed form of the perturbed distribution function, whereas the form of the distribution function did not affect this term for linear drag. In order to evaluate the viscous relaxation and collisional change of the stress tensor, we assume that the velocity distribution in the ignited state can be described by (3.6). Thus, the viscous relaxation of the stress tensor is given by

$$\langle f_D P_{ij}\rangle = P_{ij} + \lambda[p\delta_{ij} + \tfrac{34}{15}(P_{ij} - p\delta_{ij})], \tag{6.4}$$

where $\lambda = \alpha Re^{2/3} T^{1/3}$ with $Re \equiv 9(\rho_p/\rho_f)\, St$ and

$$\alpha = \frac{2^{1/3}}{\pi^{1/2}}\frac{11}{36}\Gamma(\tfrac{5}{6}) \approx 0.245.$$

Substituting (3.15) for $\partial_c P_{ij}/\partial t$ and (6.4) for $\langle f_D P_{ij}\rangle$ in the balance equation for the stress tensor (6.3), the stress tensor and temperature can be obtained

$$P_{xx} - p = \left[2(1+\lambda) - \frac{72}{35}\frac{\omega}{St}(1+\lambda)^2\right](1 + \tfrac{24}{5}St\omega + \tfrac{34}{15}\lambda)^{-1} T, \tag{6.5a}$$

$$P_{yy} - p = -\left[(1+\lambda) + \frac{72}{35}\frac{\omega}{St}(1+\lambda)^2\right](1 + \tfrac{24}{5}St\omega + \tfrac{34}{15}\lambda)^{-1} T, \tag{6.5b}$$

$$P_{zz} - p = -\left[(1+\lambda) - \frac{144}{35}\frac{\omega}{St}(1+\lambda)^2\right](1 + \tfrac{24}{5}St\omega + \tfrac{34}{15}\lambda)^{-1} T, \tag{6.5c}$$

$$P_{xy} = -\frac{3}{St}(1+\lambda)\, T, \tag{6.5d}$$

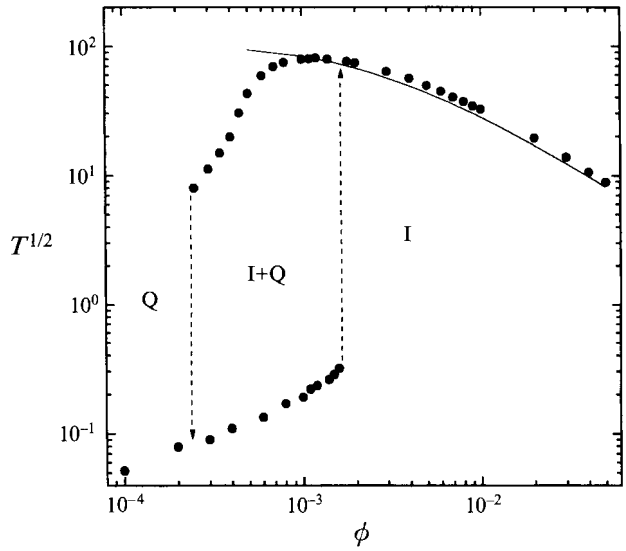


FIGURE 10. The granular temperature of the suspension with nonlinear drag is plotted as a function of the volume fraction for $St = 10$ and $\rho_p/\rho_f = 1000$.

and

$$6(1+\lambda)\left(1+\frac{24}{5}St\omega+\frac{34}{15}\lambda\right)^2-St^2\left[\frac{19}{15}\lambda+\frac{24}{5}St\omega-\frac{72}{35}\frac{\omega}{St}(1+\lambda)^2\right]=0. \qquad (6.5e)$$

Setting $\lambda = 0$, (6.5) reduces to the results (3.15)–(3.19) for Stokes drag law. No explicit analytical solution of (6.5$e$) for $T$ is possible when $\lambda \neq 0$. The moments solution is given by the lines in figures 10, 12 and 13.

To obtain an exact solution of the Boltzmann equation and detailed information on the velocity distribution function, the direct-simulation Monte Carlo method, which was introduced in §4, is used to simulate the suspension with nonlinear drag. An explicit solution for $C(t; C_0)$ from the equation of motion of the particles (6.1) cannot be obtained for the nonlinear drag law. Therefore, we adopt a second-order time-stepping scheme. On the first time step after a collision, the Euler method is used to calculate the velocities of the colliding particles.

The symbols in figure 10 represent the results of the simulation. For a suspension with Stokes drag, we had multiple steady states but no hysteresis was obtained by varying the volume fraction. The temperature in the ignited state increased monotonically as $\phi$ was decreased, as it does in rapid granular flow. For a suspension with nonlinear drag, we obtain both multiple steady states and hysteresis in the regime $\phi_{c1} \leqslant \phi \leqslant \phi_{c2}$ as shown in figure 10. When one increases $\phi$ in the quenched state for $St = 10$, the temperature grows and the system ignites at $\phi \approx 1.6 \times 10^{-3}$. As we expect, this value is close to that for Stokes drag because the nonlinear drag reduces to Stokes drag for the small Reynolds numbers encountered in the quenched suspension. On the other hand, as one decreases $\phi$ in the ignited state, a downwardly concave shape of the temperature in the ignited state is found. The temperature grows at first in a manner similar to the result for Stokes drag. Then it reaches a maximum at about $\phi = 10^{-3}$ and starts to decrease. Finally, the ignited state cannot be sustained for $\phi < \phi_{c2} \approx 2.5 \times 10^{-4}$. As $\phi$ is decreased, the mean free path $a\phi^{-1}$ becomes large. With a linear drag law, the root-mean-square particle velocity can rise sufficiently so that the collision time approaches a constant as $\phi \to 0$. In reality, however, the nonlinearity of the drag

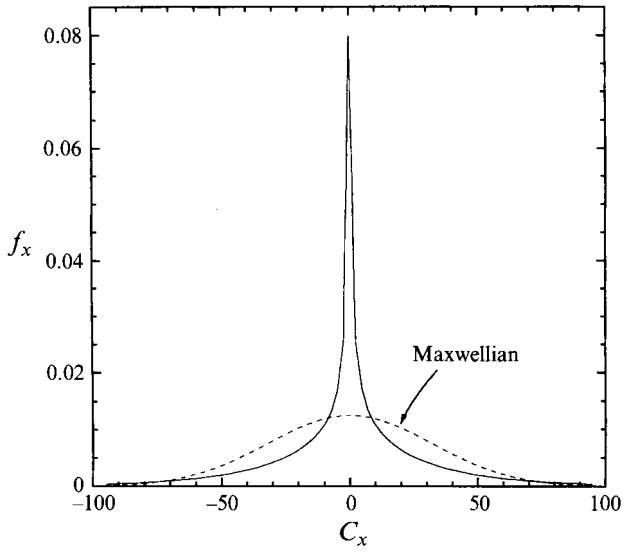


FIGURE 11. The marginal velocity distribution function $f_x(C_x)$ of the suspension with nonlinear drag for $\phi = 4 \times 10^{-4}$, $St = 10$ and $\rho_p/\rho_f = 1000$.

becomes increasingly important as the fluctuating velocities increase; this limits the growth of $T$ with decreasing $\phi$ and eventually leads to quenching. Thus, the divergence of granular temperature as $\phi \to 0$ predicted in granular flow will be eliminated if the particles experience a drag force that grows faster than linearly with particle velocity.

The velocity distribution function can be described by a perturbation from the Maxwellian due to shear flow if $\gamma\tau_c \ll 1$. For an ignited suspension with linear drag, $\gamma\tau_c$ is about $4.8/St$ and $\gamma\tau_c \ll 1$ is satisfied if $St \gg 1$. According to the simulation, the Hermite expansion is a reasonable approximation down to $St \approx 5$. This means that the perturbation scheme can be extended up to $\gamma\tau_c \sim O(1)$. With the nonlinear drag law, $\gamma\tau_c \approx 4.4$ for $St = 10$ and $\phi = 1 \times 10^{-3}$. The marginal velocity distribution, $f_x$, agrees very well with the Maxwellian for $\phi \geqslant 1 \times 10^{-3}$ and the predictions of the moment method for the temperature are accurate for these volume fractions (see figure 10).

However, the shear becomes dominant when $\gamma\tau_c > 4$. As shown in figure 10, the moment method fails to predict the decay of the temperature with decreasing $\phi$ for $\phi \leqslant 10^{-3}$. For $St = 10$ and $\phi = 4 \times 10^{-4}$, $\gamma\tau_c \approx 37.2$ which means $\tau_c/\tau_v \sim O(1)$ and the nonlinear drag term becomes more important than the collision term. Since the shear and nonlinear drag terms are dominant for $\phi < 10^{-3}$, the velocity distribution is expected to be far away from the Maxwellian. To understand this behaviour further, the marginal velocity distribution $f_x$ for $St = 10$ and $\phi = 4 \times 10^{-4}$ is given as a linear–linear plot in figure 11 and compared with the Maxwellian. $f_x$ has a peaked structure with a maximum about six times that of the Maxwellian with the same variance. However, unlike the highly peaked velocity distribution in the quenched state shown in a logarithm–linear plot in figure 5, there is still a substantial fraction of the particles with velocities much larger than $\gamma a$ in this ignited suspension with nonlinear drag.

The $\mu_p/\mu_p^*$ and the normal stress differences for a dilute ignited suspension with Stokes drag are given by expressions similar to those for a dilute gas and depend on $\phi$ only through their dependence on the granular temperature. However, the rheological behaviour of a suspension with a nonlinear drag force is unlike a dilute gas and this

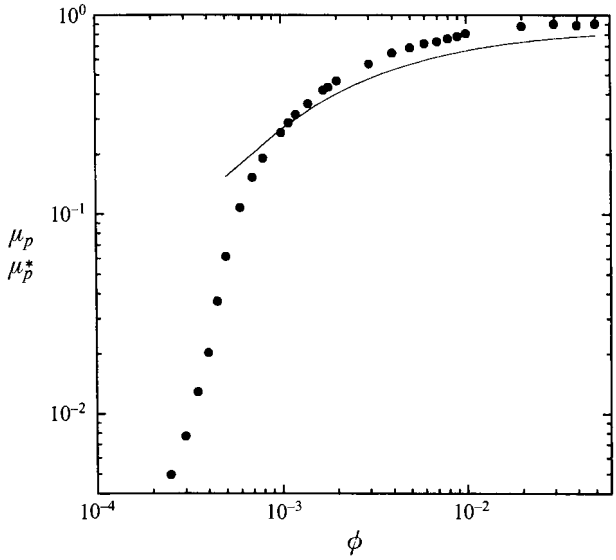


FIGURE 12. The effective viscosity of the particle phase is plotted as a function of the volume fraction for $St = 10$ and $\rho_p/\rho_f = 1000$. The line corresponds to the theoretical analysis and the symbols to the simulation results.

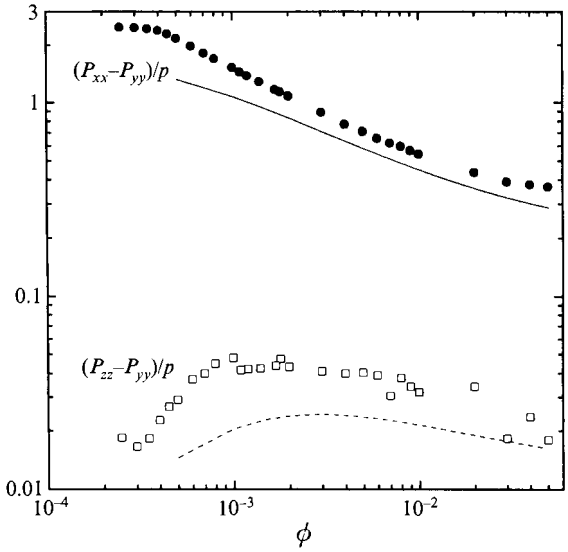


FIGURE 13. The normal stress differences are plotted as a function of the volume fraction for $St = 10$ and $\rho_p/\rho_f = 1000$. The lines are theoretical predictions and the symbols are the simulation results.

can be illustrated by the volume fraction dependence of the effective viscosity and normal stress differences shown in figures 12 and 13, respectively. As can be seen from figure 12, $\mu_p/\mu_p^*$ deviates from 1 significantly as the suspension becomes dilute and drops very quickly as $\phi \to \phi_{c1}$. The first normal stress difference in figure 13 increases as $\phi$ is decreased and reaches a maximum value of about three as $\phi$ approaches $\phi_{c1}$. This $O(1)$ first normal stress difference comes from the streaming mode which controls the velocity distribution as $\phi$ decreases toward $\phi_{c1}$. On the other hand, the second

normal stress difference is still small, $O(0.01)$, owing to the slight difference in the collisional sources of $P_{yy}$ and $P_{zz}$. A suspension with nonlinear drag behaves more like a Newtonian fluid as it becomes more concentrated. When $\phi$ increases, the temperature decreases due to frequent collisions. The effects of nonlinearity in (6.2) become smaller, and the suspension becomes more Newtonian. However, the suspension behaviour will be close to Newtonian only as long as $T \gg (\gamma a)^2$. It is this lower limit on the temperature that usually causes dense granular flows to be non-Newtonian.

In dilute granular flows of highly inelastic particles, Richman (1989) obtained analytical results for the stress tensor based on an anisotropic Maxwellian distribution of particle velocity fluctuation and showed that purely inelastic quenching does not take place in simple shear. In order to preclude the divergence of the shear stress as the particle volume fraction tends to zero, the effects of particle–wall collisions have been considered in studies of pipe flow. Invoking an analogy to the Knudsen free-molecule regime, Sinclair & Jackson (1989) replaced the mean free path $L$ in the expression for the effective viscosity by $\min(L, R)$ where $R$ is the pipe radius. Similarly, Louge *et al.* (1991) adopted the approximation $\mu_p/\mu_p^* = (1+L/R)^{-1}$. However, by introducing the effects of nonlinear drag, $\mu_p/\mu_p^* \to 0$ as $\phi \to 0$ even in an unbounded domain, i.e. $L \ll R$. Either of these mechanisms may limit the growth of $\mu_p^*$, depending on the Stokes number and the size of the domain.

## 7. Conclusion

We have explored the behaviour of a dilute gas–solid suspension subjected to a laminar simple shear flow, using numerical simulations and a kinetic theory based on a moment expansion. The suspension can exist in two very different states: an ignited state, in which the variance of the particle velocity is very large, and a quenched state, in which the particle velocity is close to the local fluid velocity. The criterion for the Stokes number, volume fraction and initial particle velocity variance leading to each of these states has been determined. Over a range of Stokes numbers and volume fractions, it is possible to obtain either the quenched or ignited state depending on the initial particle velocity variance.

We have also examined the rheology of the particle phase. In the ignited state, there are significant normal stress differences at Stokes numbers comparable to the minimum value, $St_{c1} \approx 5$, for which the ignited state can be maintained. As the Stokes number is increased, the velocity distribution approaches the Maxwellian and the rheology becomes more Newtonian. The nonlinearity of the drag when the particle Reynolds number is not asymptotically small substantially increases the non-Newtonian behaviour.

Only a small $O(St\phi)$ fraction of the particles in the quenched suspension have velocities that differ substantially from the local fluid velocity. Following a rare shear-driven collision, however, a particle may attain an $O(\gamma a St)$ difference from the fluid velocity by travelling an $O(St)$ distance in the direction of the velocity gradient. The momentum transferred by particle translation leads to an $O(St^3\phi^2)$ contribution to the effective viscosity of the suspension. However, the shear stress is always dominated by the viscosity of the gas in the quenched state, for which $St^3\phi \leqslant O(1)$.

It is interesting to note that the moment method using a Hermite polynomial expansion gives quantitatively accurate results in the ignited regime even quite close to the critical Stokes number, $St_{c1} \approx 5$, where the non-Newtonian behaviour is quite substantial (see figure 1). To show how far from the Maxwellian the distribution can be without losing accuracy in the determination of the second moment, we show the

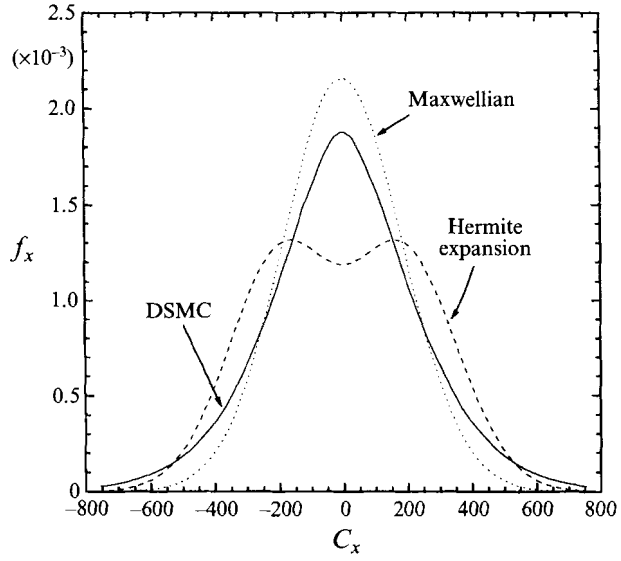


FIGURE 14. A comparison of several velocity distributions with the same second moment for $St = 5.02$ and $\phi = 0.01$. The solid line corresponds to the simulation results, the dashed line to the Hermite expansion, and the dotted line to the Maxwellian.

distribution function for $\phi = 0.01$ and $St = 5.02$ in figure 14. The solid line represents the distribution determined from numerical simulations, the dashed line the approximate distribution assumed in the Hermite expansion, and the dotted line the Maxwellian with the same second moment. The assumed distribution does not give the correct fourth- and higher-order moments. However, we noted in §3 that these moments couple weakly to the second moments and so the errors incurred in calculating the suspension rheology are small. We found that several other approaches to the kinetic theory gave the same or nearly the same results for the rheological properties and the critical Stokes number for quenching. These include a moment method based on an anisotropic Gaussian velocity distribution, a model based on analogy with Maxwell molecules in which the force constant is adjusted artificially to reflect the correct temperature dependence of the viscosity for hard spheres (Tsao *et al.* 1993), and a BGK equation with a temperature-dependent collision rate which plays a similar role.

The situation we have studied in the present work is idealized in that the suspension is dilute, gravitational forces and particle inelasticity are neglected, and the gas flow is assumed to be laminar. However, we believe that the qualitative features of our results are significant for more general gas–solid flows. In Sangani *et al.* (1995) the present results are extended to higher particle volume fractions by including the effects of hydrodynamic particle interactions. Many of the simulation results for the dense suspension are explained in terms of an extension of the present theory to include collisional stresses and volume-fraction-dependent viscous dissipation.

The kinetic energy associated with velocity fluctuations may dissipate owing to inelastic collisions. For a suspension with nearly elastic particles at a large Stokes number, the velocity distribution is close to the Maxwellian. The collisional energy dissipation per unit volume can be evaluated and is equal to $12(1-e^2)\phi^2 T^{3/2}/\pi^{1/2}$. Thus the criterion for the viscous dissipation due to Stokes drag, $3\phi T/St$, to dominate is $36/5 \gg St^2(1-e^2)$. From this criterion, it appears that inelastic effects dominate

independent of particle volume fraction at a sufficiently large Stokes number. However, this criterion only applies to an ignited suspension with $St \gg 1$ and $Re_T \ll 1$. The viscous drag plays a dominant role in the dynamics of the quenched state and in the transition between ignited and quenched states. No quenched state is observed in simulations of a dilute granular flow in the absence of drag even if the coefficient of restitution is quite small (Campbell 1989). Even in the ignited state, nonlinear drag becomes increasingly important as the volume fraction increases and the granular temperature grows, so that eventually nonlinear drag dominates as $\phi \to 0$. In Sangani *et al.* (1995), we consider the coupled effects of drag and inelasticity.

Unfortunately, it is not possible to obtain a dilute gas–solid flow in which gravity can be neglected in the presence of the Earth's gravitational force. For a solid–liquid system, negligible gravitational effects can be achieved by matching the density of the solid and fluid as in the classical experiments of Bagnold (1954). Bagnold obtained results indicating that particle inertia and interparticle collisions were dominant for $St > 22$ at the smallest volume fraction that he studied, $\phi = 0.13$. This criterion lies somewhat above our critical Stokes number of 5. However, the strong lubrication forces and increased form drag in a liquid–solid suspension in addition to the inelasticity of the wax particles used in the experiments could easily account for this difference. It would be quite straightforward to include inelastic effects in the present theory, but the complications of liquid inertia and lubrication pose considerable difficulties.

A microscopic kinetic-theory analysis of gas–solid suspensions can be performed for simple flows and simple models of the solid-body particle interactions. A phenomenological continuum description which can be formulated for more complex situations is useful for qualitative understanding and for engineering applications (Goddard 1986). For $St \gg 1$, as shown in (3.29), the constitutive relation for the stress tensor is Newtonian. For a finite-$St$ suspension in the absence of particle density variation and conduction of granular temperature, (2.7) and (3.7) may be combined to construct an 'Oldroyd'-like constitutive equation for the stress tensor (Bird, Armstrong & Hassager 1977):

$$\tau\left(\frac{D\hat{\boldsymbol{P}}}{Dt}+\boldsymbol{W}\cdot\hat{\boldsymbol{P}}-\hat{\boldsymbol{P}}\cdot\boldsymbol{W}\right)+\tau(\widehat{\hat{\boldsymbol{P}}\cdot\hat{\boldsymbol{D}}}+\widehat{\hat{\boldsymbol{D}}\cdot\hat{\boldsymbol{P}}})+\hat{\boldsymbol{P}}=-2p\tau\hat{\boldsymbol{D}}, \tag{7.1}$$

where $1/\tau = 2/\tau_v + \omega^{(2,2)}$. $\boldsymbol{W}$ is the vorticity tensor and $\hat{}$ denotes the deviatoric of a tensor. The quadratic terms in the collisional change of the second moment have been neglected. The term on the right-hand side shows a temperature (shear-rate)-dependent viscosity. The term in parenthesis on the left-hand side of (7.1) is the change of the stress tensor as witnessed by an observer translating and rotating with the flow. Note that (7.1) must be supplemented by the energy balance

$$\rho_s\frac{\mathrm{D}T}{\mathrm{D}t}+\tfrac{2}{3}\hat{\boldsymbol{P}}:\hat{\boldsymbol{D}}+\frac{2}{\tau_v}\rho_s T=0. \tag{7.2}$$

From the continuum viewpoint, the multiplicity of steady states obtained in the present study may be viewed as a natural consequence of the nonlinearity associated with the dependence of the stress $\boldsymbol{P}$ on the shear rate $\gamma$ and the temperature $T$ and it is likely that such a multiplicity may be obtained for a wider range of conditions than those studied in the present physical model of gas–solid suspensions. However, multiplicity of steady states is not present in the standard theory of rapid granular flow and one requires an appropriate kinetic model to predict the presence or absence of the quenched/ignited transition in any specific physical system.

The authors wish to thank A. S. Sangani for helpful discussions. The work was supported by the National Aeronautics and Space Administration Microgravity Program (NAG3-1630) and by the Office of Naval Research (N00014-91-J-1790).

## REFERENCES

ALFONSO, M., GAÑÁN-CALVO, A. M. & LASHERAS, J. C. 1991 The dynamics and mixing of small spherical particles in a plane, free shear layer. *Phys. Fluids* A **3**, 1207–1217.

BAGNOLD, R. A. 1954 Experiments on a gravity-free dispersion of large solid spheres in a Newtonian fluid under shear. *Proc. R. Soc. Lond.* A **225**, 49–63.

BIRD, G. A. 1970 Direct simulation and the Boltzmann equation. *Phys. Fluids* **13**, 2676–2681.

BIRD, R. B., ARMSTRONG, R. C. & HASSAGER, O. 1977 *Dynamics of Polymeric Liquids*. John Wiley & Sons.

BRINKMAN, H. C. 1947 A calculation of the viscous force exerted by a flowing fluid on a dense swarm of particles. *Appl. Sci. Res.* A **1**, 27–34.

CAMPBELL, C. S. 1989 The stress tensor for simple shear flows of a granular material. *J. Fluid Mech.* **203**, 449–473.

CAMPBELL, C. S. 1990 Rapid granular flows. *Ann. Rev. Fluid Mech.* **22**, 57–92.

CHAPMAN, S. & COWLING, T. G. 1970 *The Mathematic Theory of Non-Uniform Gases*, 3rd edn. Cambridge University Press.

CLIFT, R., GRACE, J. R. & WEBER, M. E. 1978 *Bubbles, Drops, and Particles*. Academic.

EINSTEIN, A. 1906 Eine neue Bestimmung der Moleküldimensionen. *Ann. Phys.* **19**, 289–306 (see also **34**, 591–592, 1911).

ELGHOBASHI, S. E. & ABOU-ARAB, T. W. 1983 A two-equation turbulence model for two-phase flow. *Phys. Fluids* **26**, 931–938.

GODDARD, J. D. 1986 Dissipative materials as constitutive models for granular media. *Acta Mechanica* **63**, 3–13.

GOLDREICH, P. & TREMAINE, S. 1978 The velocity dispersion in Saturn's rings. *Icarus* **34**, 227–239.

HERDEGEN, N. & HESS, S. 1982 Nonlinear flow behavior of the Boltzmann gas. *Physica* **115A**, 281–299.

HOPKINS, M. A. & SHEN, H. H. 1992 A Monte Carlo solution for rapidly shearing granular flows based on the kinetic theory of dense gases. *J. Fluid Mech.* **244**, 477–491.

JENKINS, J. T. & RICHMAN, M. W. 1988 Plane simple shear of smooth inelastic circular disks: the anisotropy of the second moment in the dilute and dense limits. *J. Fluid Mech.* **192**, 313–328.

JENKINS, J. T. & SAVAGE, S. B. 1983 A theory for the rapid flow of identical, smooth, nearly elastic particles. *J. Fluid Mech.* **130**, 187–202.

KOCH, D. L. 1990 Kinetic theory for a monodisperse gas–solid suspension. *Phys. Fluid* A **2**, 1711–1723.

KUMARAN, V., TSAO, H.-K. & KOCH, D. L. 1993 Velocity distribution functions for a bidisperse, sedimenting particle–gas suspension. *Intl J. Multiphase Flow* **19**, 665–681.

LOUGE, M., MASTORAKOS, E. & JENKINS, J. T. 1991 The role of particle collisions in pneumatic transport. *J. Fluid Mech.* **231**, 345–359.

LUN, C. K. K., SAVAGE, S. B., JEFFREY, D. J. & CHEPURNIY, N. 1984 Kinetic theories for granular flow: inelastic particles in Couette flow and slightly inelastic particles in a general flow field. *J. Fluid Mech.* **140**, 223–256.

MAXEY, M. R. 1987 The motion of small spherical particles in a cellular flow field. *Phys. Fluids* **30**, 1915–1928.

MEI, R. & ADRIAN, R. J. 1992 Flow past a sphere with an oscillation in the free-stream velocity, and unsteady drag at finite Reynolds number. *J. Fluid Mech.* **237**, 323–341.

LAWRENCE, C. J. & MEI, R. 1995 Long-time behaviour of the drag on a body in impulsive motion. *J. Fluid Mech.* **283**, 307–327.

RICHMAN, M. R. 1989 The source of second moments in dilute granular flows of highly inelastic spheres. *J. Rheol.* **33**, 1293–1306.

SANGANI, A. S., MO, G.-B., TSAO, H.-K. & KOCH, D. L. 1995 Rapidly sheared, dense gas–solid suspensions. *J. Fluid Mech.* (submitted).

SAVAGE, S. B. & JEFFREY, D. J. 1981 The stress tensor in a granular flow at high shear rates. *J. Fluid Mech.* **110**, 255–272.

SINCLAIR, J. L. & JACKSON, R. 1989 Gas–particle flow in a vertical pipe with particle–particle interactions. *AIChE J.* **35**, 1473–1486.

SQUIRES, K. & EATON, J. K. 1990 Particle response and turbulence modification in isotropic turbulence. *Phys. Fluids* **A 2**, 1191–1203.

TSAO, H.-K., KOCH, D. L., MO, G.-B. & SANGANI, A. S. 1993 Inertial effects in suspensions. In *Proc. 5th NSF-DOE Workshop on Fluid Solids Transports, Ithaca, NY,* pp. 121–130.

ZWANZIG, R. 1979 Nonlinear shear viscosity of a gas. *J. Chem. Phys.* **71**, 4416–4420.